الجمهورية الجزائرية الديمقراطية الشعبية

PEOPLE'S DEMOCRATIC REPUBLIC OF ALGERIA

وزارة التعليم العالي والبحث العلمي

Ministry of Higher Education and Research

University Saad Dahlab Blida 1

Institute of Aeronautics and Space Studies

Aeronautical Construction Department

Final Master's Thesis

To obtain the diploma of

Master in Aeronautics

Option : AVIONICS.

THEME

Inspection and detection of photovoltaic system faults by drone.

Directed by :   *Accomplished by :*

Dr. KOBZILI Elhaouari,   Mlle. MECHREF Milissa,

Dr. KRIM Mohamed .   Mlle. REGGANI Soultana.

Sustained in front of the jury composed of :

Pr. BENKHEDDA Amina.	*Professor*	*President*
Dr. OTMANE Fadhéla.	*MCA*	*Examiner*
Dr. KRIM Mohamed.	*MCB*	*Examiner*

Promotion : 2022 / 2023

Dedication

We dedicate this modest work to:

First and foremost, to those who cannot be compensated for the sacrifices they

have made for our education and well-being - our parents. They have selflessly

taken care of us throughout our education and are the reason behind our success.

May God bless and protect them.

To our REGGANI, MECHREF, and BERRAKI families, as well as our dear

friends, who have provided us with support during the most challenging moments.

Acknowledgement

Resume

➢ **Arabic :**

الاطروحة الموسومة بعنوان "تفتيش وكشف الأعطال في أنظمة الطاقة الشمسية بواسطة الطائرة بدون طيار" تتضمن دراسات نظرية حول أنظمة الطاقة الشمسية والطائرات بدون طيار، بالإضافة إلى تطبيقاتها في هذا المجال. تقدم المذكرة كل من الأساليب التقليدية والمبتكرة لتفتيش أنظمة الطاقة الشمسية وتحاكي بنجاح سلوك هذه الأنظمة.

هذه المذكرة تشمل الحل المقترح المناسب باستخدام الطائرات بدون طيار للقيام بعملية فحص المصفوفات الكهروضوئية تبعا لمسارMATLAB محدد يتم محاكاته ببرنامج .

لاكتمال هذه العملية يتطلب معالجة الصور المأخوذة لهذه الالواح الشمسية من خلال مقارنتها مع مجموعة بيانات شاملة على مختلف العيوب المحتملة وتحديد هذه الاخيرة بالضبط

وتوصلت الاطروحة إلى أن الحل المقترح فعال في اكتشاف الأعطال في الأنظمة الكهروضوئية، وهو أمر حاسم لصيانتها وأدائها المناسبين مما يجعل الطائرات بدون طيار ثورة في مجال الطاقة الشمسية

➢ **English :**

The master thesis titled "Inspection and Detection of faults of Photovoltaic Systems by Drone" explores the utilization of drones for inspecting and detecting faults in photovoltaic systems. The thesis encompasses theoretical studies on photovoltaic systems and drones, as well as their applications in this domain. It presents both traditional and innovative inspection methods for photovoltaic systems and successfully simulates the behavior of these systems.

The proposed solution involves deploying a drone to inspect photovoltaic arrays, generating its trajectory using MATLAB, and employing image processing techniques of captured drone images to detect malfunctions based on a dataset.

The thesis concludes that the proposed solution is effective in identifying faults, which is of utmost importance for maintaining and improving the performance of photovoltaic systems.

> **French:**

Le mémoire de de fin d'études intitulé "Inspection et détection des pannes des systèmes photovoltaïques par drone" explore l'utilisation des drones pour inspecter et détecter les défauts dans les systèmes photovoltaïques. Le mémoire comprend des études théoriques sur les thématiques citées plus haut, ainsi que leur éventuelle application dans ce domaine. Il présente à la fois des méthodes d'inspection traditionnelles et innovantes pour les systèmes photovoltaïques et simule avec succès le comportement de ces derniers.

La solution proposée implique le déploiement d'un drone pour inspecter les panneaux photovoltaïques, générer sa trajectoire à l'aide de MATLAB et utiliser des techniques de traitement d'images des images capturées par le drone pour détecter les dysfonctionnements sur ses dernières basées sur une dataset d'un ensemble de données.

Le mémoire conclut que la solution proposée est efficace pour identifier les défauts, ce qui est d'une importance capitale pour maintenir et améliorer les performances des systèmes photovoltaïques.

List of abbreviations

AIRT: Aerial Infrared Thermography

°C: Celsius Degrees

CNN: Convolutional Neural Network

DC: Direct Current

DIP: Digital Image Processing

EL: Electroluminescence Imaging

°F: Fahrenheit Degrees

HT: Italian company selling electrical instruments

I-V: Current-Voltage

IRT: Infrared Thermography

MPP: Maximum Point Power

MW: Mega Watt

PV: Photovoltaic

RGB: Red Green Blue colour model

SCADA: Supervisory Control And Data Acquisition

STC: Standard Test Conditions

SUNSPEC: Alliance setting industry standards by establishing technical specifications

UAV: Unmanned Aerial Vehicle

μm: Micrometre

Voc: Open Circuit Voltage

LIST OF SYMBOLS

SYMBOL	DESCRIPTION	UNIT
x, y, z	Cartesian coordinates	m
$\dot{x}, \dot{y}, \dot{z}$	Translation velocity	m/sec
$\ddot{x}, \ddot{y}, \ddot{z}$	Translation accelerations	m/sec^2
ϕ, θ, ψ	Euler angles (Roll, Pitch, Yaw)	Rad
$\dot{\phi}, \dot{\theta}, \dot{\psi}$	Angular velocity	Rad/sec
$\ddot{\phi}, \ddot{\theta}, \ddot{\psi}$	Angular acceleration	Rad/sec^2
V	Vector of linear velocities	---
$q=\{\phi,\theta,\psi,x,y,z\}$	Vector of generalised coordinates	---
m	Quadrotor's mass	kg
d	Distance between the centre of quadrotor's gravity and the axis of rotation of the propellers	m
g	Acceleration of gravity	m/sec^2
ω_i	Angular velocity of rotor i	Rad/sec
Γ_i	The moments applied to the quadrotor structure	N.m
k_p	Coefficient of lift	N.s^2/rad^2
Ω	Angular velocity expressed at the marker linked to the centre of the quadrotor	---
μ	Luminance	nit
σ	Contrast	---
C_1, C_2	constant to ensure stability when the denominator becomes 0	---

Summary

List of figures

List of tables

General Introduction

General Introduction:

The human desire to fly has been a persistent dream throughout history. This aspiration led to significant advancements in aviation technology, opening up new possibilities for exploration and development. The aeronautics industry has existed for many years and continues to develop rapidly, serving as an essential tool in transportation as well as military applications. However, the influence of this lasts was not limited to these areas only; it extends across other domains.

However, the use of manned aircraft is not always practical or cost-effective for certain tasks like inspection or surveillance purposes, leading to the development of unmanned aerial vehicles (UAVs) or drones. Equipped with advanced sensors and cameras, these latter machines are able to collect high-resolution images from multiple angles without the need for physical contact based on the equipment making them suitable tools for identifying corrupt things in different places.

Recently, technological developments have focused on developing more efficient and environmentally friendly solutions. This has led - lately in some countries to increase their interest in renewable energy sources, especially solar energy. In this context, Algeria is among the many nations that have recognized the potential of renewable energy in promoting sustainable development efforts. With an abundance of solar sources, this country has invested heavily in large-scale photovoltaic systems. The use of this source is designed to capture solar irradiation and convert it into electricity. However, like any other electrical system, photovoltaic systems are vulnerable to faults that can lead to significant power loss or complete failure resulting from many causes such as pollution and hot spots, making their detection essential to ensure optimum performance and prevent potential defects.

During this study, an issue was identified. Which is centered on exploring strategies for integrating UAV technology into photovoltaic systems to improve fault detection capabilities and the challenge involved identifying a reliable methodology for detecting faults in this last using drones.

To address these challenges, the master's thesis proposes an investigation into the feasibility of utilizing drone technology for inspecting large-scale photovoltaic systems. This would involve equipping installations with cameras capable of capturing high-quality images of photovoltaic panels and leveraging image-processing algorithms to detect any potential faults or anomalies affecting system performance. By implementing such an approach, we can significantly enhance our ability to monitor and maintain renewable energy infrastructure while promoting sustainable development efforts globally through effective

monitoring mechanisms leading towards cost savings while reducing carbon emissions affecting our environment positively.

In the proposed study, we developed a conceptual model for an efficient and cost-effective detection system that uses drone technology to inspect and detect faults in photovoltaic systems. The research seeks to integrate this approach with advanced image processing techniques, resulting in a solution capable of accurately identifying any potential malfunctions or anomalies present within photovoltaic arrays.

Organization of the dissertation

This dissertation is organized into four chapters as follows:

➤ The first chapter presents an overview of fundamental research in the field of photovoltaics, emphasizing the principle of the photovoltaic effect. Additionally, we will present an overview of drones and their flight principle.

➤ In the second chapter, we present an extensive examination of various detection methods for photovoltaic faults will be presented, with a specific focus on the methods employed in our project.

➤ In chapter three, we describe the methodology used to gain a better understanding of inspection areas by simulating desired systems.

➤ The final chapter offers a comprehensive study that includes drone simulation using MATLAB and proposes a solution that highlights an innovative approach put forward in our research.

At the conclusion of this master's thesis, we will provide a general conclusion consisting of a summary of our work and different perspectives concerning future developments in this field.

Chapter 1

Drones and photovoltaic systems,

a theoretical study

CHAPTER 1: DRONES AND PHOTOVOLTAIC SYSTEMS, A THEORETICAL STUDY.

1.   INTRODUCTION:

The upcoming chapter will be split into two sections. Initially, we will introduce renewable energies and specifically solar energy in Algeria, then we will define the photovoltaic effect, its system, its operating mechanism, and potential malfunctions.

In the second section, we will provide a concise summary of the navigation field concerning quad rotors, including the progression, advancements, and categorization of unmanned aerial vehicles. Following that, our investigation will concentrate on a particular type of small drone, the quad copter. We will explore some research studies that operate in this research area, focusing on the principle of flight, their field of application, and the limitations we can find.

2.   RENEWABLE ENERGY:

Renewable energy refers to energy sources that can naturally be restored and can be repeatedly utilized without depleting their resources and without harming our environment which makes it an eco-friendly source and an adequate solution to the depletion of fossil energy sources. Indeed, they come from natural elements: sun, wind, waterfalls, and tides…, The imperative for global adoption of this energy has been significantly amplified due to escalating concerns surrounding climate change and the urgent necessity to transition towards a low-carbon economy [1]. This brings us to the advantages of these sources such as reduced greenhouse gas emissions, improved air quality, and decreased dependence on imported fossil.

Figure 1.1 Renewable energy [2].

2.1   Algeria's renewable energy potential:

2.1.1 Solar energy:

Due to its strategic geographical location, Algeria presents substantial promise as a viable region for the exploitation of solar energy resources. Notably, it exhibits exceptionally high solar irradiance levels, positioning it among the global front-runners in this regard. The solar irradiance measurements indicate a remarkable capacity of generating an estimated range of 1,850 to 2,100kilowatts per hour , making Algeria an attractive prospect for solar energy development and deployment. as the figure below shows [3].
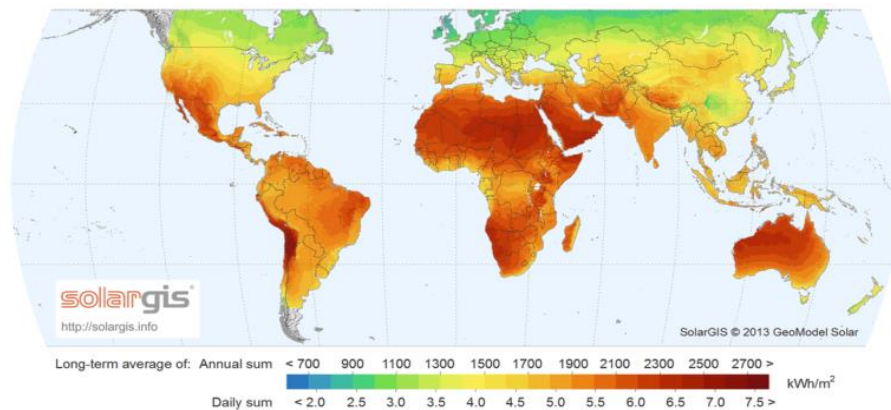
Figure 1.2 : Solar irradiance around the world [4].

When we take a closer look at the global irradiation in Algeria we can notice that in some regions it can reach 2410 Kwh/m² which is a huge and important number in the solar energy field as the figure shows.
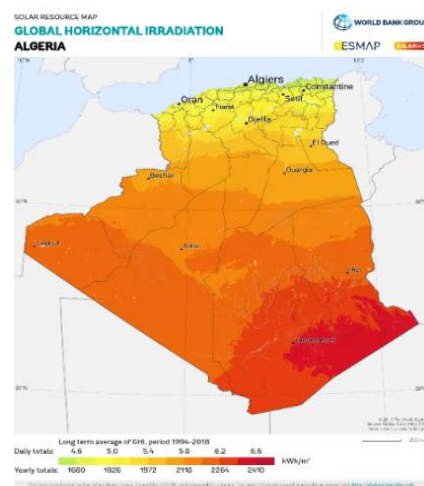
Figure 1.3 : Global horizontal irradiation in Algeria [5].

And for that, Algeria has conceived a very ambitious program to develop this energy during the period 2015-2030, it consists of installing a total capacity of 22,000MW, of which the photovoltaic system will be the main source of energy production. In fact, the photovoltaic system represents 62% of the total capacity projected by 2030 as the **figure 1.4** shows [6].
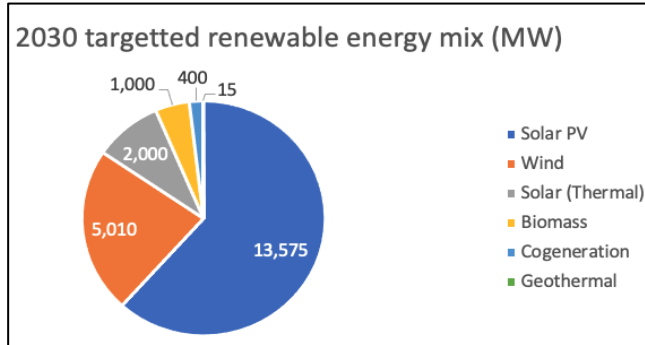
Figure 1.4 : The Algerian's renewable energies [7].

However, Algeria has already many photovoltaic power plants with different capacities, the figure below shows the photovoltaic power plants realized by Sonelgaz.
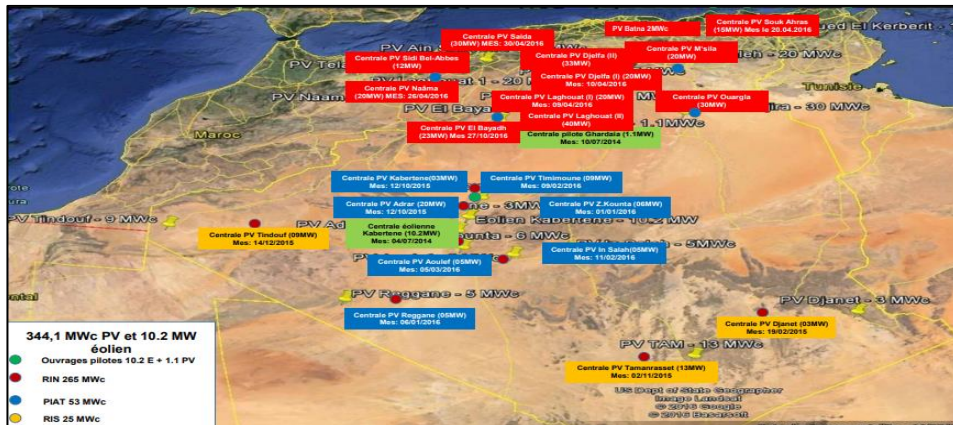
Figure 1.5 : Photovoltaic power plants around Algeria [8].

Zooming on some of the solar power plants:

Figure 1.7 : Photovoltaic power plant with a capacity of 5 MW in Reggane, Adrar [9].

Figure 1.7 : Photovoltaic power plant with a capacity of 20 MW in Adrar [9].

3.   PHOTOVOLTAIC SYSTEM:

3.1   Definition of a photovoltaic system:

Before getting into the definition of a photovoltaic system, we should first know what photovoltaic means.

The term "photovoltaic" originates from the Greek words for "light" and the name of Italian physicist Alessandro Volta in (1745–1825), who is renowned for his discovery of the electrochemical battery and after whom the unit of electric potential, the Volt, is named [10]. He discovered the first functional electrochemical battery and the unit of electricity, Volt, is named after him. Thus, a translation of the word photovoltaic could be a light battery or also a light source. More generally we understand the word photovoltaics as the direct conversion of sunlight into electric energy [10].

Photovoltaic systems offer a clean, quiet, and dependable method for generating electricity. These systems are comprised of photovoltaic devices and cells that directly convert light energy into electrical energy, and since the primary source of light is typically the sun, these devices are commonly referred to as solar cells [11].

A photovoltaic system can consist of various components, including solar panels, batteries, regulators/controllers, inverters, and chargers, as illustrated in Figure.
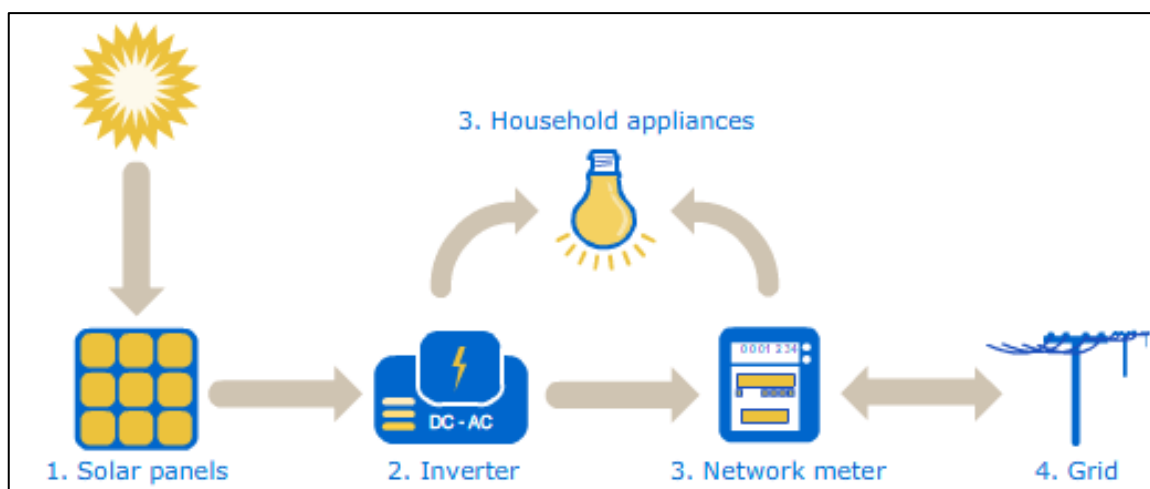
Figure 1.8 : how a solar system works [12].

3.2   History of solar energy:

Here are some important dates about the historical path of solar energy [13]:

➢   **1839:** The process of utilizing sunlight to generate an electric current within a solid material was discovered by the esteemed French physicist, Edmond Becquerel.

➢   **In 1875**, Werner Von Siemens presented an article on the photovoltaic effect in semiconductors to the Berlin Academy of Sciences. But until the Second World War, the phenomenon remains a laboratory curiosity.

➢   **1954:** Three American researchers, Chapin, Pearson, and Prince, develop a high-efficiency photovoltaic cell at a time when the emerging space industry is looking for new solutions to power its satellites.

➢   **1958:** A cell with a yield of 9% is developed. The first satellites powered by solar cells are sent to space.

➢   **In 1973:** The first house powered by photovoltaic cells is built at the University of Delaware.

➢   **In 1983:** In Australia, a significant milestone in the field of photovoltaic energy was achieved when the inaugural car powered solely by solar energy traveled an impressive distance of 4,000 km.

Today, photovoltaic technology continues to evolve and improve, with ongoing research focused on increasing efficiency, reducing costs, and developing new materials and applications. The photovoltaic industry is now a major player in the global energy sector, providing an increasingly significant share of the world's electricity supply.

3.3   Photovoltaic effect:

The photovoltaic effect is the physical phenomenon where light (photons) is absorbed by a semiconductor material, which creates a flow of electrons that can be harnessed to generate electrical power.

In a photovoltaic cell, this is achieved by creating a p-n junction (a boundary between two regions of semiconductor material with different doping levels) that separates electrons and holes [14].

When a photon is absorbed by the cell, it generates an electron-hole pair, which is then separated by the built-in electric field of the junction. The electrons flow towards one electrode and the holes towards the other, generating an electric current. By connecting multiple cells in series, the voltage can be increased to generate useful power [14].

3.4   Photovoltaic cell:

A photovoltaic (PV) cell, also known as a solar cell, is a specialized device that converts sunlight directly into electrical energy through the photovoltaic effect as illustrated in (**Figure 1.9**).
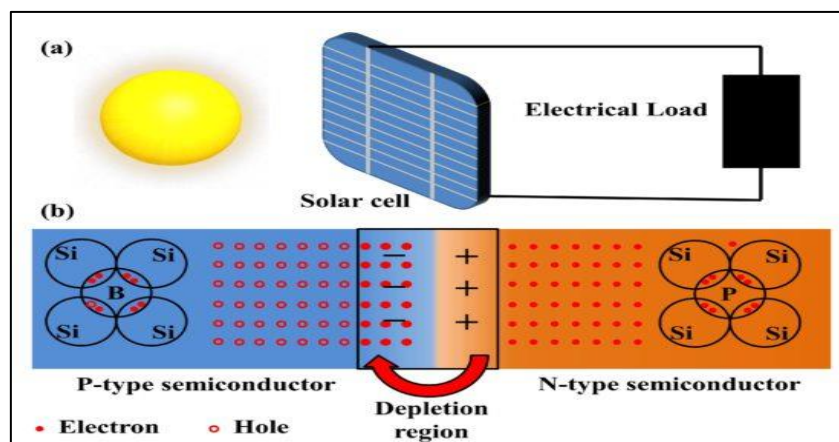
Figure 1.9 : (a) Conversion of solar energy through solar cells. (b)
A visual depiction of the p-n junction and depletion region [15].

3.4.1 principle of a photovoltaic cell:

A solar cell has to be designed such that the electrons and holes can reach the membranes before they recombine, i.e. the time it requires the charge carriers to reach the membranes must be shorter than their lifetime. This requirement limits the thickness of the absorber [16].
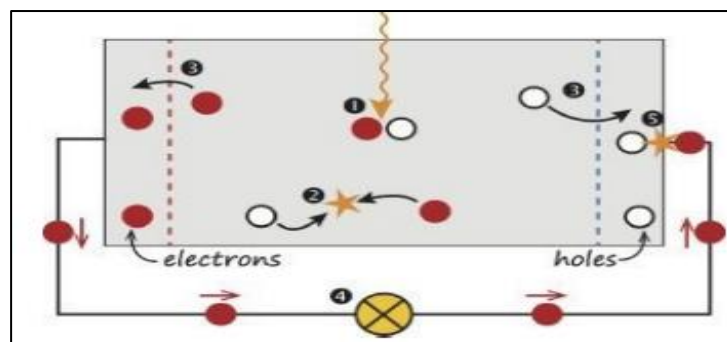
Figure 1.10: A very simple solar cell model [16].

According to the figure upward [16]:

1. The absorption of a photon leads to the generation of an electron-hole pair.
2. Usually, the electrons and holes will recombine.
3. With semipermeable membranes the electrons and the holes can be separated.
4. The separated electrons can be used to drive an electric circuit.
5. After the electrons have passed through the circuit, they will recombine with holes.

3.5   Photovoltaic module:

The module is a set of photo batteries (cells) assembled to generate usable electrical power during its exposure to light [11]. For almost all applications, the voltage produced by a single cell is insufficient so to solve this problem and produce more power, solar cells are assembled in series, and that will increase voltage for the same current while paralleling increases current by maintaining voltage [11].
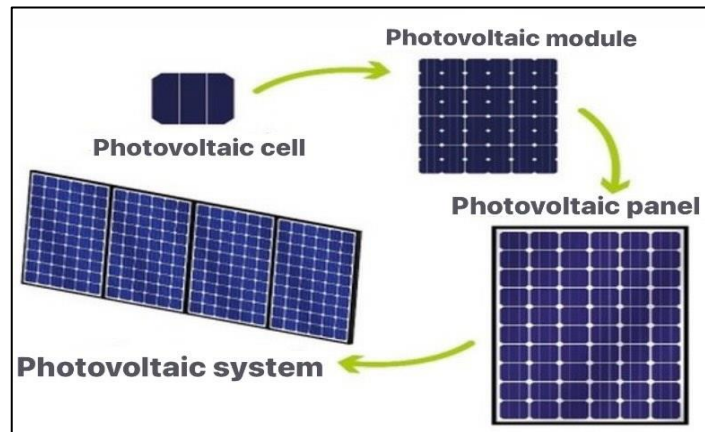
Figure 1.11: Going from a photovoltaic cell

to a panel field [17].

3.6   Faults and failures of photovoltaic systems:

Photovoltaic systems are subjected to a variety of faults that can impact the energy production, and the safety of the system, it can also lead to a loss in the economic benefits of the system [18].

Failure in general terms is explained as an effect that degrades the ability of a system and cannot be inverted by normal operation [19]. The same scenario applies here with the photovoltaic systems. Any abnormal operation that occurs under normal operation of a PV module is relevant for the warranty and is termed as a photovoltaic module or system failure [19]. **Table 1** depicts some very serious faults that occur in photovoltaic systems.
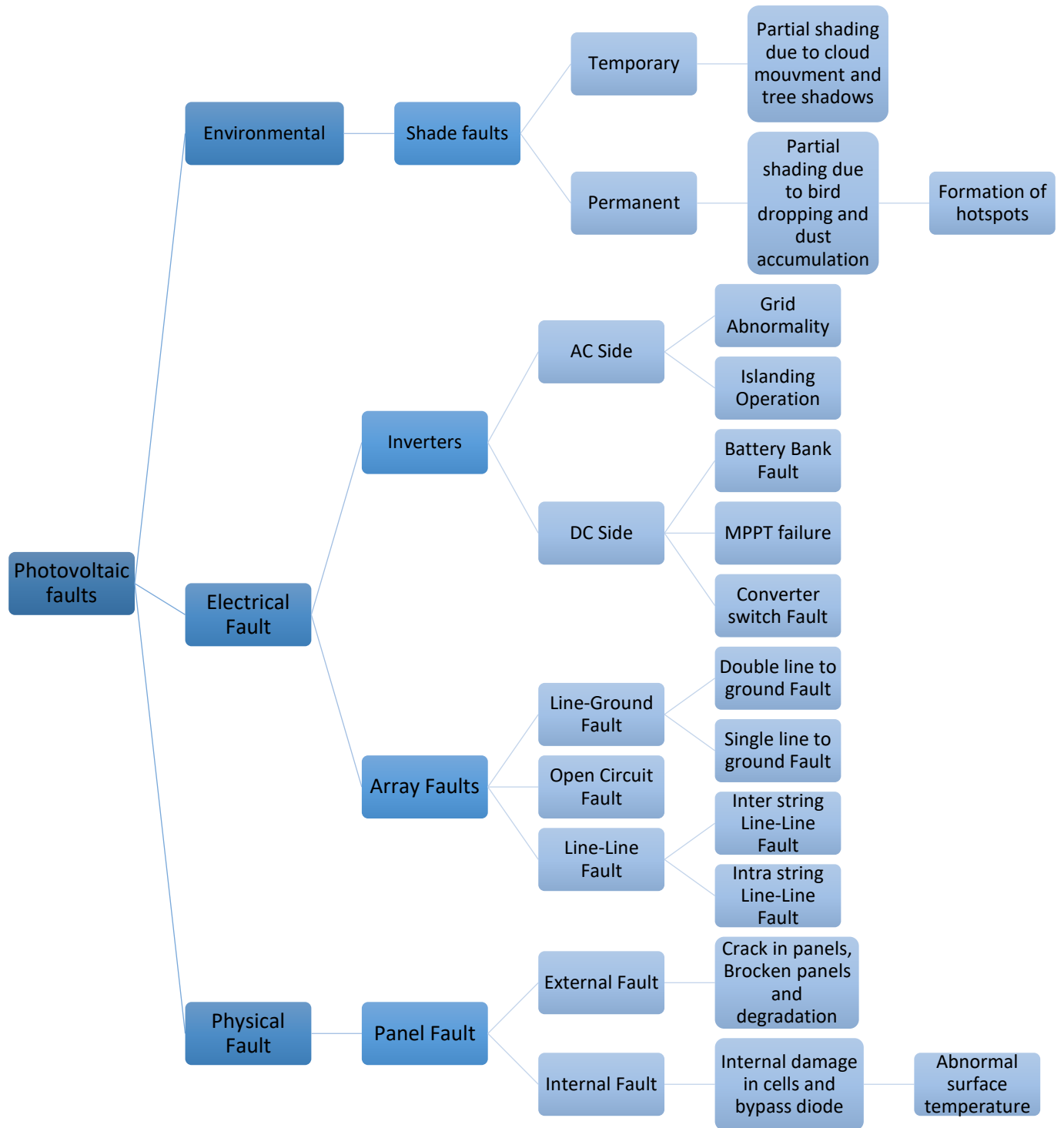
Table 1.1: Faults in a photovoltaic system [18].

4.   A SUMMARY OF UNMANNED AERIAL VEHICLES:

4.1   Definition of drone:

A drone, also known as an unmanned aerial vehicle (UAV), is an aircraft that doesn't require a human pilot on board. The drone can fly with different levels of autonomy, either controlled remotely by a human operator or independently through onboard computers. [20]. Drones are classified into different categories based on their broad applications, and from the design perspective, generally fall under three major groups: military, industry, and commercial [20].

4.2   History of drones:

Drones and quadcopters have a rich history. With the help of advanced computer technology and engineering, their development has been rapid and their impact on many industries, including defense, agriculture, mapping, surveillance, and exploration, is significant.

1783 – The First UAV

Hot-air balloons are often overlooked or excluded from discussions surrounding unmanned aerial vehicles (UAVs). These airplanes were the first in terms of technology to fly without a human pilot. The first public display of an unmanned aircraft, a hot air balloon, was presented by Joseph-Michel and Jacques-Étienne Montgolfier in Annonay, France [21]. The Austrian artillery officer Franz von Uchatius created a balloon bomb which was utilized by Field Marshall von Radetsky to attack Venice, although they were largely ineffectual. As you can see in (**figure1.12)** bellow:

Figure 1.12 : incendiary balloons which were used by Australia
against Venice in 1849 [22].

Some of these balloons worked, while the wind blew others back into Austrian territory [23]. When compared to the technologically advanced UAVs of today, they may not be on par in terms of technological capabilities.

After World War I, unmanned aircraft known as planes without pilots began to emerge. Among these was the Hewitt Sperry Automated Airplane, which Elmer Sperry of the Sperry Gyroscope company developed and later became the precursor to today's aerial torpedo [23].

The American military repurposed Standard E-1 planes into drones, such as the Larynx where this small monoplane had the capability to fly autonomously once deployed from a warship. [23]. Other automated aircraft were developed by the US and British military.

Reginald Denny, a prosperous Hollywood actor with a passion for remote-controlled drones, pioneered the first mass-produced airplane. He established Reginald Denny Industries, which created the radio plane that he subsequently enhanced for use by the American military during World War II. The US military then experimented with these remote-controlled drones and produced various aerial torpedoes utilized as target drones during the Cold War. Furthermore, these drones were capable of collecting radioactive data.

The first quadcopters

The quadcopter configuration is a prevalent characteristic of numerous contemporary commercial drones[21]. This technology's initial development dates back to 1907, when brothers Jacques and Louis Bréguet collaborated with French physiologist Professor Charles Richet to produce a gyroplane, which was a precursor to the helicopter and featured the quadcopter layout[21]. As you can see in **Figure 1.13** below:

Engineers started developing quadcopters after the gyroplane to address the challenges that helicopter
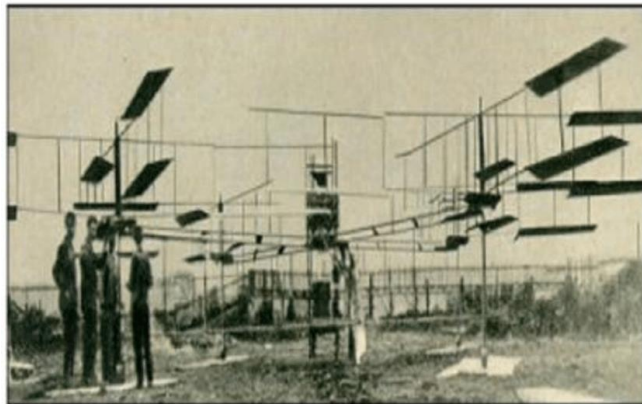
Figure 1.13 : first Gyroplane (1907) [24]**.**

pilots faced while making vertical flights. The first of these was the Omnichen 2, invented by Étienne Omnichen in 1920 [23].

The Convertawings Model a quadcopter, as depicted in **Figure 1.14**, was designed by Dr. George E. Bothezat and made its debut in 1956. It was the first quadcopter to utilize propulsion, or the forward thrust generated by a propeller, to regulate the aircraft's roll, pitch, and yaw. The Curtis Wright V27, developed by the Curtis Wright Company, followed suit in 1958 [23].
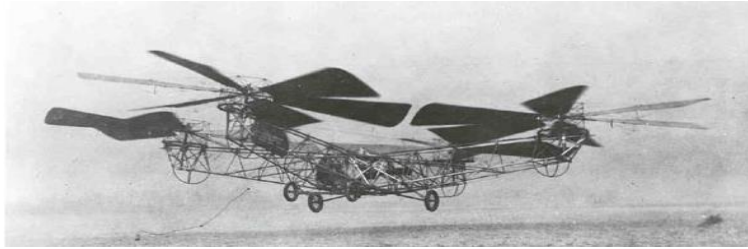
Figure 1.14 : Bothezehat Helicopter (1923) [25].

The aircraft completed 1,000 successful flights and covered a recorded distance of 360 meters (1,181.1 feet)

ver the last few decades, numerous miniature rotary-wing drones have been developed for civil applications and utilized by scientists. Many of these drones have been successfully marketed, including the Draganflyer, Parrot's AR. Drone 2 and Bebop 2, DJI's Phantom and Mavic models, and Gaui 330X, among others [26].

The impact of drones on civil society has provided numerous advantages that have improved human living conditions. Consequently, this topic has attracted the attention of industries, R&D centers, and universities worldwide, which are now tackling new challenges like obstacle detection and avoidance, control, vision landing, localization techniques, data fusion, and more. A recent study presented the various experimental platforms of drones. Indeed, technological advancements in electric motors, batteries, embedded electronic systems, and wireless communication have facilitated the development of several prototypes ranges [26].

Figure 1.15 : Example of nowadays
drones, Parrot Bebop2 [27].

4.3   Classification of drones:

Drones exist in different sizes, capabilities and a wide variety of models "For that many classifications have been proposed to distinguish existing systems based on their operational characteristics and capabilities [28]. As the figure below shows, we will focus on

13

a specific classification based on the drone's size, range, endurance, number of rotors, and altitude.

UNMMANED AERIAL VEHICLES TYPES			
	SIZE	Micro UAV	200g or less
		Mini UAV	200-1000g
		Medium UAV	1-20kg
		Large UAV	20kg
	RANGE	Very Low-cost Close Range	distance of 5km for 1h of flight
		Close Range	distance up to 50km for 1 to 6h of flight
		Short Range	distance up to 15km for 8 to 12h of flight
		Mid Range	distance of 644km for 24h of flight
	ALTITUDE	LADP	Low altitude deep penetration : 50-9000m
		LALE	Low altitude long endurance : 3000m
		MALE	medium altitude long endurence : 3000m
		HALE	High altitude long endurence : 20.000m
	ROTORS	Singe Rotor	
		Multi Rotor	

Table 1.2: Classification of Unmanned Aerial Vehicle types drones based on size, range, number of rotors, and altitude[29].

4.4   Quadcopter drone:

A quad-copter is a specific type of drone with 4 rotors. In other words, it is a rotary-wing aircraft equipped with four arms, each of it is connected to a motor. The rotors are generally positioned at the ends of a cross-shaped configuration[30]. However, the presence of a qualified pilot is necessary, especially for the delicate phases of
flight: take-off or landing[31].

These quadcopters have been so successful for some time since it is an innovative technology that allows us to obtain shots and videos[31].

4.4.1 Principle of flight of a quadcopter:

The process of piloting a quadcopter involves the task of maintaining the aircraft on its designated trajectory, while appropriately managing and regulating any alterations to the trajectory in either the vertical or horizontal plane[31]**.** For that, we need to look at its dynamics and rotor motion.

4.4.1.1   Inertial and body frame:

In order to in to have a good understanding of how a quadcopter flies, a definition of the frames is required.
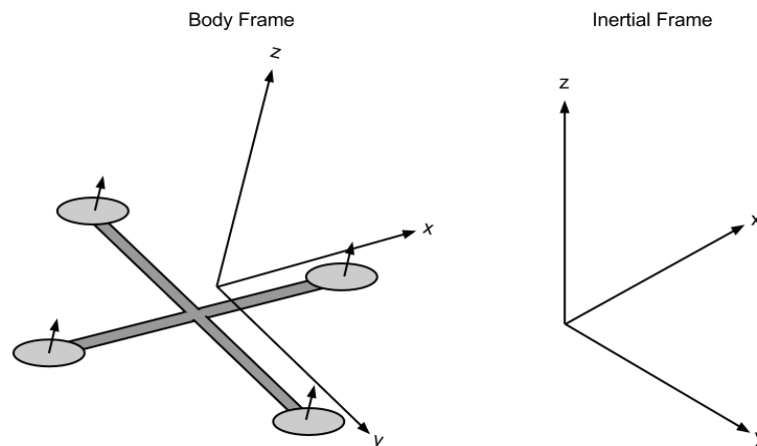
Figure 1.16 : Quadrotor body frame and inertial frame [32].

The body frame is related to the quadcopter's orientation while the inertial frame is established by the ground, with gravity being oriented in the negative z-direction as it is shown upward in (**Figure 1.16**) [33]**.**

4.4.1.2   Quadcopter dynamics:

The quadcopter has 6 degrees of freedom. This means that 6 variables are needed to express its position and orientation in space (x, y, z, φ, θ, and ψ) [34].

The x, y, and z variables represent the distances of the quadcopter's center of mass along the x, y, and z axes respectively from the fixed reference frame.

The movement of a quadcopter is based on the force exerted on each propeller and it is classified into four types of movements based on the other three variables known as Euler angles which represent the quadcopter orientation and they are:

- The pitch angle: (θ) is the angle about the y-axis.
- The roll angle: (φ) is the angle about the x-axis.
- The yaw angle: (ψ) is the angle about the z-axis.
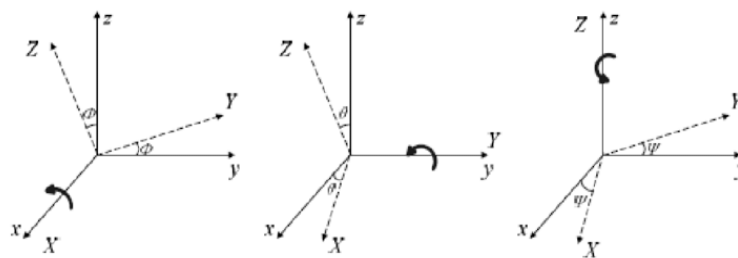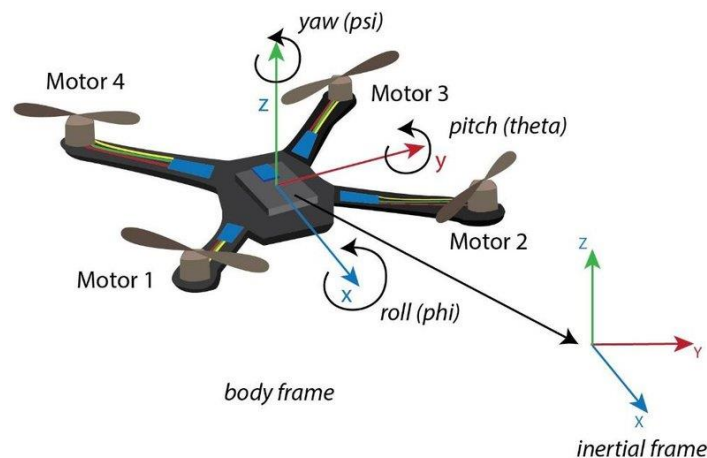
Figure 1.17 : Quadrotor in the body frame and Euler angles representation [35].

When it comes to the most important thing in the quadcopter's principle of flight, we need to avoid the device from rotating on its yaw axis, two propellers must rotate in one direction, while the other two rotate in the opposite direction as the (**Figure 1.17**) shows.
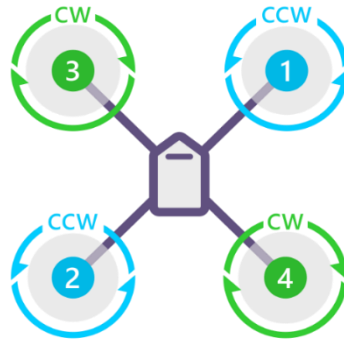
Figure 1.18 : quadrotor saw from the top
and its propeller's rotation direction [36].

A drone can perform four primary movements, which are:

• **Hover:** The ability to move up and down, and for that To move down the four propellers need to run at a normal speed.

• To move upward the four propellers have to increase the speed.

➢ **Pitch:** Pitching motion which is the ability of the drone to move forward or backward (the y-axis)

• To move forward the rotation speed of helices 1 and 3 must be decreased, while those of helices 2 and 4 must be increased [31]. This action will cause the quadcopter to lean forward.

• To move backward we reverse the rotation speed of the forward motion.

➢ **Roll:** Rolling motion is the ability of the drone to move right and left (the x-axis)

• To move right the rotation speed of helices 2 and 3 must be decreased, while those of helices 1 and 4 (the two left propellers) must be increased [31]. This action will cause the quadcopter to lean to the right.

• To move left we reverse the rotation speed of the right move so we increase the rotational speed of the two right propellers.

➢ **Yaw:** Yawing motion which is the ability of the drone to rotate either left or right (z-axis)

• When two propellers on the right diagonal of a drone rotate at a high speed while the other two on the left diagonal remain stationary, the drone will start to rotate in an anti-clockwise direction (to the left) [31].

• If the opposite happens, the drone will start to rotate in a clockwise direction (to the right)
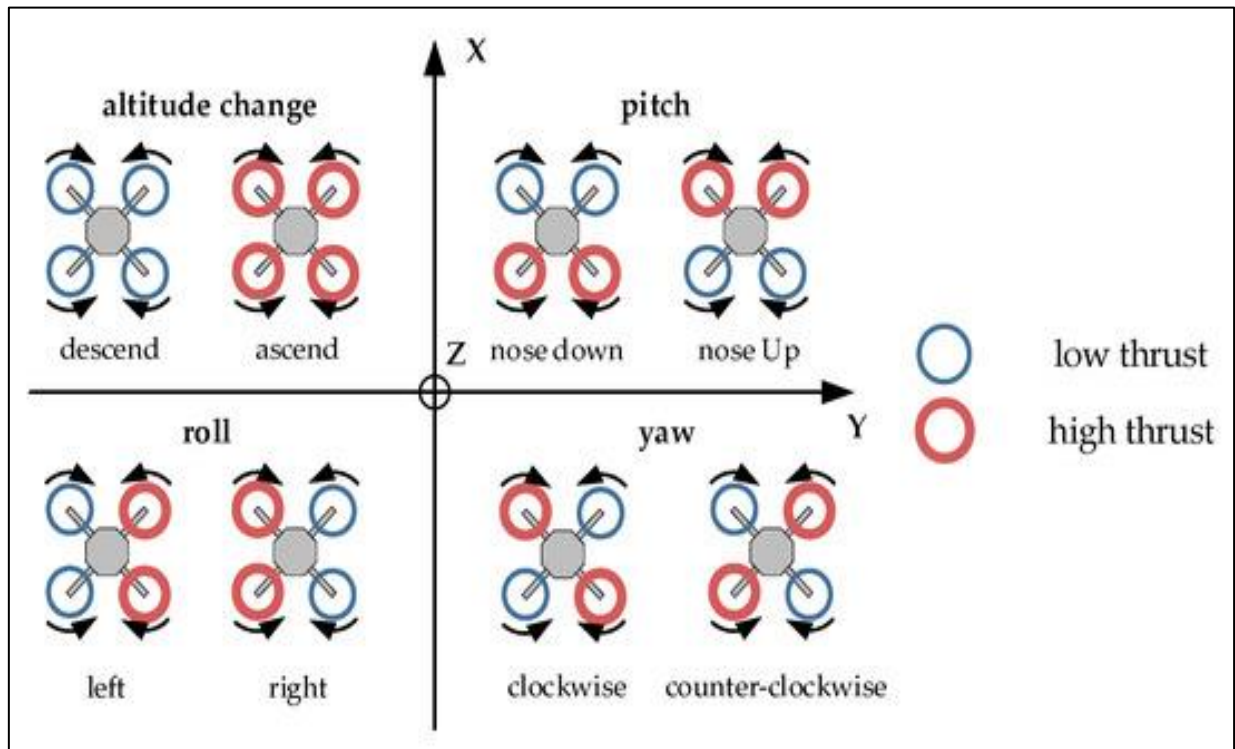
Figure 1.19 : Basic principles of quadcopter maneuvering [36].

4.4.2 Quadcopter applications:

Quadcopters have revolutionized our world by providing us with a glimpse into the future with their small dimensions and high maneuverability. They can perform functions that may be difficult or time-consuming for humans to accomplish. This has opened up a wide range of possibilities in various industries, including agriculture, transportation, and surveillance. One of the most important applications of quad copters is the following:

4.4.2.1   Military applications:

➢   **Reconnaissance and surveillance area:** Drones are equipped with advanced optical sensors that allow them to gather vast amounts of information about potential targets. These sensors are capable of capturing high-resolution images and videos, providing valuable insights into enemy activities and movements.

➢   **Direct support for fighting and training tasks:** Drones equipped with missiles can give significant help in fights due to their high precision. They can also be a part of training tasks like surveying the militants.

> ➤ **Conducting the shares of intelligence:** Drones can operate in environments that may be too dangerous or difficult for human operatives to access. They are also highly maneuverable and can cover large areas quickly, providing a wide range of surveillance options.

> ➤ **Tracking a moving target:** Drones can provide real-time data on the target's speed, direction, and location, allowing military forces to plan and execute tactical maneuvers more effectively.

4.4.2.2   Civilian applications:

> ➤ **Science and research:** Drones can be used in monitoring, diagnostics, and analytics of level gases emission, fumes, and other harmful or undesirable substances [37].

> ➤ **Inspections:** checking many systems such as power lines, wind turbines, and pipelines [38].

> ➤ **Unmanned cargo system:** They can serve in delivering lightweight packages to customers [38].

> ➤ **Fire brigade:** thermal imaging cameras mounted on drones can detect hot spots, even through smoke and darkness, and provide valuable information to firefighters on the ground and detect fire sources. In another hand, drones can track and monitor the sources of pollution [38].

> ➤ **Renewable energy:** Drones can provide considerable help in the field of renewable energies, and that's by inspecting the material as photovoltaic panels and wind turbines which reduce a considerable amount of time and effort for the employees.

4.4.3 Risks associated with the use of drones:

Even with all the good sides of using drones, we can't close our eyes to the risks those devices have. Here are the most important risks:

> ➤ **Collision Risk:** Drones can collide with obstacles (trees, buildings, high-voltage lines).
> ➤ **Discharge the battery.**
> ➤ **Damage caused by weather conditions**: (low air temperature, precipitation).

These three risks can be predicted; therefore action should be taken to prevent their uprising. The battery status and other telemetry data, including temperature can be controlled remotely by the system [37]. In case of exceeding one of the parameters, the alarm should be launched and this will allow take the action, such as an emergency recall of the drone to a branch. However, the sensors and software that are based on the flight path and the detected obstacles continuously update the route and are responsible for the avoidance of obstacles [37].

➤ **Privacy Risks**: These devices can follow tracked objects and observe them from many different perspectives. They can be equipped with cameras, night vision devices, and various sensors, facilitating snooping. While their wide use by municipal services (including the police) to control the civilian population could pose a danger to human rights [37].

➤ **Security Risks**: Drones can be used to deliver contraband, such as drugs or weapons. As we saw in the military applications, drones can be used as weapons themselves which is for the benefit of the country, but this ability can be used in a risky way, either by terrorists or other malicious actors.

➤ **Cybersecurity Risks:** Drones are increasingly connected to the internet, which makes them vulnerable to cyber-attacks and can be hacked which makes them weak and sensitive pieces of information can be stolen.

By utilizing quadcopters, we can enhance efficiency and productivity while reducing costs and saving time. Their versatility and adaptability have made them valuable assets in numerous applications, allowing us to achieve feats that were previously considered impossible.

4.5   The use of drones in the photovoltaic field:

Drones, also known as unmanned aerial vehicles (UAVs), have transformed many industries due to their versatility and efficiency. One such industry is the photovoltaic solar energy sector, where drones have become indispensable tools for inspection and maintenance. The use of drones in PV inspection has not only improved accuracy and efficiency but has also reduced the risks associated with manual inspection methods.

When it comes to the working area of the photovoltaic field, detecting their faults takes time, and some of them can only be detected in specific conditions like temperature and weather, which makes it difficult to detect in a short time. That's where the drones come into work, those small devices can optimize a considerable amount of time and be so efficient by reducing man's errors, etc...

4.5.1 Advantages of using drones for PV inspection:

➤ **Improved security:** Traditional PV inspection methods necessitate technicians climbing onto rooftops or other elevated areas to inspect solar panels manually. Drones eliminate the need for workers to physically reach these locations. Dangerous zones, lowering the likelihood of accidents and injuries.

➢ **Increased efficiency:** Drones can inspect large-scale solar installations quickly, allowing for the rapid identification of issues that may require attention. This rapid assessment process reduces downtime and enables problem resolution, resulting in increased energy production and lower maintenance costs.

➢ **Better data collection:** Because drones are equipped with advanced sensors and imaging equipment, they can capture high-resolution images and thermal data, allowing for a more accurate assessment of PV panel performance and potential defects. With this improved data collection capability, solar installations can be precisely monitored and maintained.

4.5.2 The challenges of using drones in photovoltaic inspections:

Despite these advantages, there are challenges associated with integrating drone technology into photovoltaic systems.

➢ **Technical Limitations:** Drones rely on advanced sensors, robust communication systems, and precise navigation skills. Factors such as weather conditions, battery life, and payload capacity can affect performance and reliability.

➢ **Data processing and analysis**: The large amount of data generated by drone inspections requires efficient algorithms and machine learning techniques to identify patterns, trends, and anomalies that could indicate potential problems.

5.   CONCLUSION:

In summary, when used properly, drones offer significant benefits in optimizing the performance of solar power systems. Despite some challenges, the integration of this cutting-edge technology has the potential to make the solar industry more efficient, safer, and cost-effective. As drone technology and its related applications evolve, so does its potential to revolutionize the renewable energy sector. Next chapter will talk about fault detection methods.

Chapter 2

2

Faults detection methods of photovoltaic systems

Chapter2: Faults detection methods of photovoltaic systems

1. Introduction:

Photovoltaic Industries as suppliers of innovative technologies strive for solar PV monitoring, end-to-end quality assurance services, and convenient, reliable, and legally compliant monitoring solutions are essential for PV operators. In order to achieve the highest profitability from photovoltaic power plants, reliable operation, and forecasting are two important conditions, and they represent the only way to ensure that the generated energy is marketed as effectively as possible. While fault detection is also necessary because the rate of energy production can deteriorate dramatically, due to a solar panel failure as mentioned in chapter1. There are many techniques currently taking care of this.

PV faults & categories of detection methods

These methods of inspection are divided into manual, automatic, and other techniques using artificial intelligence, which will be explained in this chapter as follows:

➢ The Visual inspection
➢ PV check instruments
➢ PV weather stations
➢ Thermal Imaging
➢ Electroluminescence
➢ Neural network classification
➢ Segmentation using RGB camera

The following table represents the PV faults & categories of detection methods

Category	Methods	Defects and failures detected
Manual	The Visual inspection	Delamination, Bubbles, Cracking, Yellowing, Discoloration, Oxidation, Cell breakage
Automatic	PV check instruments	Shading, Hot spots, Snail trails
	PV weather stations	Hot spots, Soiling
Artificial intelligence	Thermal Imaging	Snail trails, Shading, Hot spots, Micro cracks, Corrosion of connectors
	Electroluminescence	Microcracks, Cell cracks, Soldering defects, Diode failure, Dead cell, Back sheet scratches, Wafer defects
	Neural network classification	Hot spots, Disconnected substrings, Open strings
	Segmentation with RGB camera	Shadings, Cell breakage, Snail trails, Delamination, Discoloration, Burn marks

Table 2.1: PV faults & categories of detection methods

2.   MANUAL TECHNIQUES:

2.1   The Visual inspection:

This method is considered the first and the most primitive operation of inspection. Visual inspection is a simple technique through which the validity of photovoltaic panels is confirmed and faults represented in cracks or dust are observed, and the electrical installation is also monitored. The most important advantages of this examination are that it does not require advanced technology, not even equipment only physical effort to carry out this process.

Figure 2.1 : *Visual inspection [39].*

While this process, although it does not require equipment or devices, will be very expensive to do so, especially for photovoltaic stations, because it needs a large number of engineers. That is why recently in order to gain time and inspect all the photovoltaic surfaces, drones are used with RGB cameras.

Figure 2.2: Visual inspection using a drone with RGB camera [40].

3.   AUTOMATIC TECHNIQUES:

3.1   PV check instruments:

Local personnel may face challenges when attempting to identify and describe the state of the PV system, potentially feeling intimidated or lacking the necessary skills to take appropriate action and it is therefore recommended to provide adequate, user-friendly instrumentation that is easy to read and understand [41]. Moreover, ensuring the availability of long-term spare parts and adequate tools is also critical for the maintenance of the PV system [41].

If a module fails during the operation of a photovoltaic (PV) plant, the system's performance may be negatively impacted. This can result in lower-than-expected efficiency, making it crucial to troubleshoot the system [42].

To ensure commissioning tests, performance recording, and troubleshooting, various measuring devices are employed.

3.1.1 The PV Tester:

PV Check multifunction device is a vital instrument in the solar energy field. It is used to measure several important specifications, including open circuit voltage, short circuit current, maximum power, the voltage at maximum power, current at maximum power, solar irradiation, and display of IV characteristics. Additionally, it can also measure series resistance, which is important for identifying the modules.

Figure 2.3 : *Digital multimeter*   **Figure 2.4 :** *HT Multifunction PV tester [43].*

The PV multifunction instrument is a versatile tool that allows users to check the safety, parameters, and performance of a PV panel. It is capable of carrying out a performance analysis of the PV array (DC) while it is operating under normal conditions, connected to the inverter [44]. The instrument provides an indication of the power generated by the PV system and the efficiency of the PV field, which depends on the irradiation condition and temperature measured by the instrument [44]. By analyzing these parameters, the PV multifunction instrument can provide valuable insights into the performance of the PV system and help users optimize its performance.

The task of this instrument here is to compare the test results with the Standard Test Conditions to see if they match each other or not and in case, this indicates that there is an issue in the PV module.

Standard Test Conditions (STC) are used to determine the power output of solar panels. Under Standard Test Conditions, solar panels are tested at 25°C (77°F) and exposed to 1,000 watts per square meter (1 kW/m^2) of solar irradiance when the air mass is at 1.5 [45].

An example of PV characteristics and STC label:

Figure 2.5: Monocrystaline panel
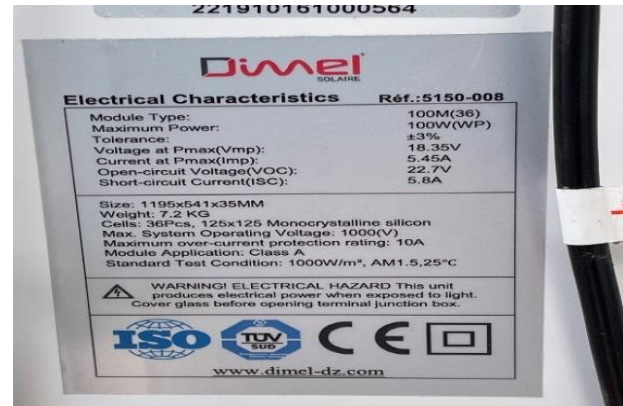
Figure 2.6: Monocrystaline panel characteristics

3.1.2   The meter IV curve Tracer:

I-V curve tracing is a method used to evaluate the performance of solar PV modules and string inverter systems. It is a reliable and efficient technique that is commonly used by solar PV installers for real-time monitoring and evaluation of module performance [46].
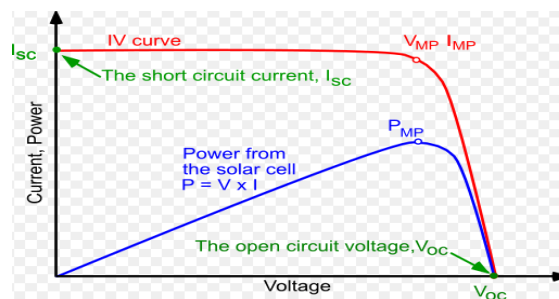
Figure 2.7: I-V Curve presentation [47].

An I-V curve tracer is a device that can quickly and accurately measure the I-V curve of a solar PV module under different irradiance and temperature conditions. It can provide important information about the module's performance, such as open circuit voltage (Voc) and the maximum power point (MPP). By comparing the I-V curves of a module over time, it is possible to diagnose any degradation in power output and identify potential issues with the module or system [48]. The use of an I-V curve tracer can save time and improve the accuracy of measurements compared to using separate instruments such as a digital multimeter, clamp meter, and irradiance meter [48].

Why are I-V curve measurements important?

By regularly screening PV modules with I-V curve tracing, any faults or issues can be identified and addressed before they become major problems. This ensures that the PV system operates efficiently and generates reliable power over its lifespan [48].

Figure 2.8: I-V Curve tracer & PV multifunction tester

3.2   PV weather stations:

Weather conditions can have a significant impact on PV output, and it's important to monitor these conditions to understand how they affect the performance of the PV system for example, changes in temperature can affect the efficiency of solar cells, while cloud cover can reduce the amount of incident solar energy [50]. By monitoring weather conditions accurately, it's possible to identify trends and patterns in PV performance and optimize the system accordingly [50].

Figure 2.9: PV weather stations installed in a PV ground [51].

PV weather stations are meteorological monitoring systems that installed in the PV grounds in order to collect weather information; wind speed, wind direction, atmospheric Temperature, atmospheric humidity, atmospheric pressure, total solar radiation and rainfall by different sensors fixed on these stations.

The following table represents the different sensors attached on PV weather stations :

Sensors	Functions
Pyranometer	An irradiance sensor for highly accurate measurement of global radiation and irradiation at module plane.
Compact weather station	Used to measure air temperature, relative humidity, solar irradiance, air pressure, wind direction and wind speed.
Wind sensor	Sensors for measurement of wind direction and wind speed.
Rain gauge	Record rain data and transmit rainfall information.
Station box	Individually configurable metrological control cabinets for central data recording and communication prewired and installed in a casing for indoor or outdoor use.
The data logger	Record all relevant system data, provide various interfaces and functionality for power plant control and thus enable grid-compliant feed-in for PV systems.

Table 2.2: Sensors attached on PV weather stations [52].

Other sensors are fixed on PV modules:

➢ **Soiling sensor:** Optical soiling detectors are a recent trend in evaluating the impact of soiling on PV systems [53]. These sensors use independent light sources to estimate the losses from optical measurements of a PV glass coupon, which means they do not require sun radiation to operate because the intensity of the light source is known, so reference measurements are not necessary, and soiling losses can be obtained instantaneously [53]. This technology provides a quick and easy way to monitor the impact of soiling on a PV system and can help optimize cleaning schedules to maintain optimal performance.

Figure 2.10: DUSST soiling sensor fixed on PV
panel [54].

➢ **Back-of panel Temperature sensor:**

Measuring PV module temperature is an important step in determining the effect of heating on the performance of a PV plant, temperature sensors are commonly attached to the back of one or more modules [55].

Figure 2.11: *Back-of PV panel Temperature
sensor [56].*

According to International Electrotechnical Commission (IEC61724-1), the number of temperature sensors required for a PV plant depends on the system size, where the table below shows the recommended number of sensors based on the system size: including signal conditioning, must be ≤ 2 °C [55].

PV plant size (AC)	Number of sensors
< 5 MW	6
≥ 5 MW to < 40 MW	12
≥ 40 MW to < 100 MW	18
≥ 100 MW to < 200 MW	24
≥ 200 MW to < 300 MW	30
≥ 300 MW to < 500 MW	36
≥ 500 MW to < 750 MW	42
≥ 750 MW	48

Table 2.3: Number of Temperature sensors according to PV plant size [57].

How does the monitoring station work?

By combining weather analytics and PV panel conditions with PV production data, solar energy output can be maintained and improved; it highlights the convenience of using modular, plug-and-play weather stations that are SunSpec certified/compliant for easy integration of important weather analytics and PV panel conditions into a SCADA system [58]. This integration allows for real-time monitoring and analysis of data, which can help optimize energy production and identify potential issues proactively [58].

Data from the weather station, inverters, combiner boxes, meters, and transformers will be collected in data loggers and passed to a monitoring station, typically via communication cables.
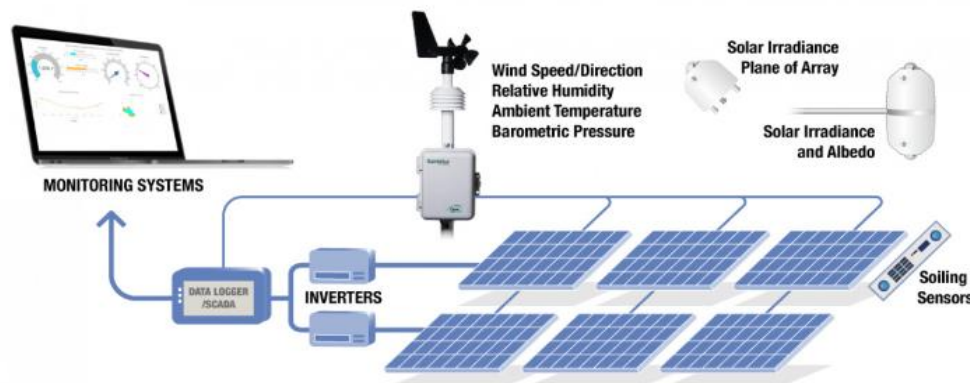
Figure 2.12: *The process of PV weather station monitoring system [58].*

In large-scale solar PV power plants, monitoring voltage and current occurs at the inverter, combiner box, or string level while inverter-level monitoring is the easiest to install, it only provides a high-level overview of the plant's performance [60]. Alternatively, combiner box and string level monitoring, though costlier, offer detailed information on component performance and significantly improve fault detection and identification capabilities [60].

4.   TECHNIQUES USING ARTIFICIAL INTELLIGENCE:

4.1   Imaging techniques:

4.1.1 Electroluminescence:

Electroluminescence (EL) imaging is a valuable tool for analyzing solar cells, offering insights into solar panel modules including solar cell characteristics, materials, health status, defects, and more [61]. The information derived from solar panel images serves as a crucial resource for applications like fault detection assessment in photovoltaics [61]

Electroluminescence (EL) is a phenomenon where photons are produced as a result of excess electron-hole pairs generated by an externally applied bias [62]. It involves the recombination of an excited electron from the conduction band to an unoccupied state in the valence band, known as a hole [63]. When individual atoms combine to form a crystal structure, the discrete energy levels of the atoms merge, forming a continuous energy level known as a level continuum [63].

Electroluminescence-imaged modules are divided into individual cells by utilizing projections along the x and y axes, enabling the detection of cell boundaries [64]. The emission of photons occurs as a result of the energy released during electron-hole recombination, and these photons, which disperse, are captured by appropriate digital cameras [65].
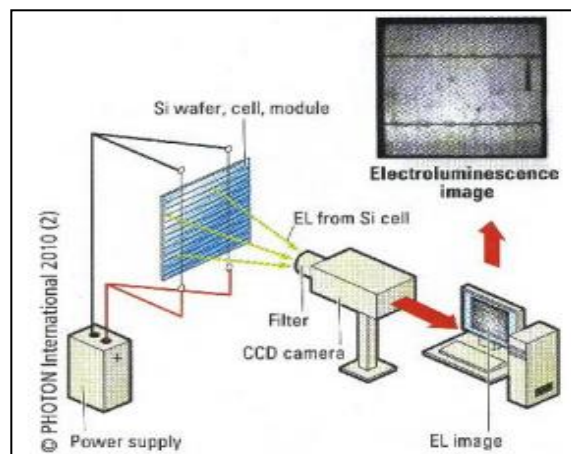
Figure 2.13: Typical Setup for EL Test *[66].*

By employing this approach, even the tiniest micro cracks on photovoltaic panels are made visible, allowing for the identification of a wide range of defects and degradation [67]. Electroluminescence (EL) imaging is capable of detecting various types of flaws in both monocrystalline and polycrystalline photovoltaic panels where these defects encompass cracks, fractures, finger interrupts, soldering issues, moisture-induced deformations, shunt faults, and disconnected components [67].
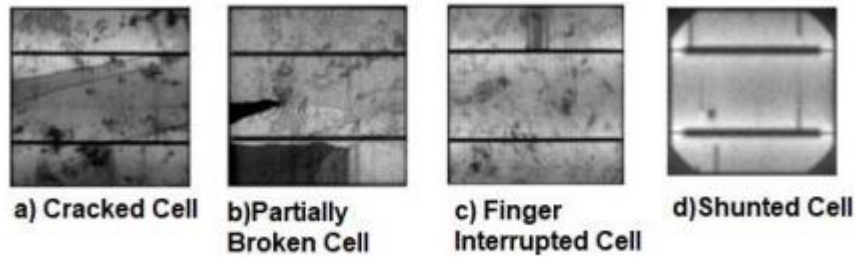
Figure 2.14: EL Images of a Various Cell Defects [68].

4.1.2 Thermal Imaging:

Studies show that thermal cameras and imaging systems are the most commonly used technology for PV monitoring [69]. Infrared thermography, which measures emitted energy from a surface, is an effective non-destructive testing technique that provides reliable temperature values at a suitable inspection rate [69]. Thermal imaging cameras convert radiation into images with temperature represented by a color scale, IR thermography is significant in PV maintenance as it can detect various faults that exhibit distinctive thermal patterns, such as hot spots and cracked silicon wafers [69].

4.1.2.1   Infrared thermography:

IRT is a technique that evaluates radiation emitted by an object within the infrared wavelength spectrum; IRT cameras used for PV inspections measure wavelengths in the mid-infrared range of 7-14 µm, which is cost-effective and practical [70]. Damaged cells and modules in a PV plant have an elevated temperature, appearing as a "temperature signature" in IRT images [71]. This technique is a reliable and non-destructive for detecting faults in PV cells, modules, and strings that affect the thermal behavior of PV modules [71].

In thermo-vision analysis, it is necessary to respect the position of the camera: [71]

➢   Choose camera height (hc) so that view angle to normal of y<40° glass surface.

➢   A too high position causes self-reflections and should be aware about

➢   other kinds of reflections such as clouds houses trees.
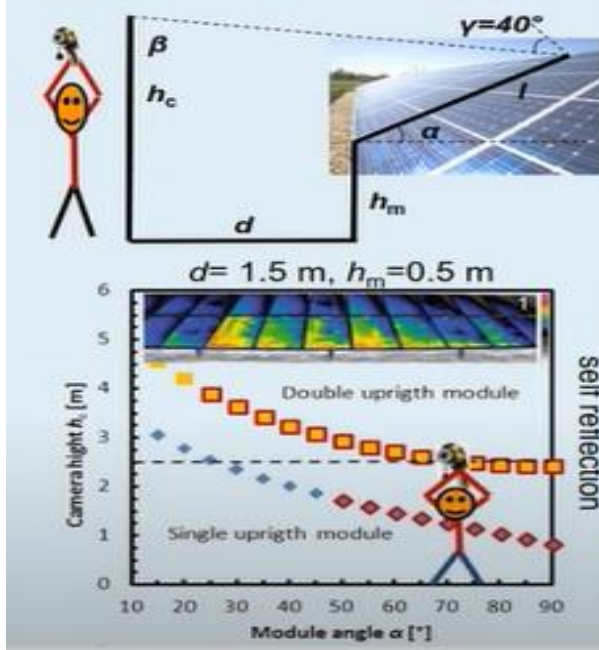
Figure 2.15: Conditions of taking Infrared
Images [71].

These manual procedures heavily rely on human labor and expertise because Ground-based or elevated IRT inspections of PV systems are typically conducted using handheld IRT cameras, which pose limitations in terms of speed, accuracy, and coverage of the entire power plant [70].

4.1.2.2   Aerial infrared thermography:

Recently, there has been growing interest from both academic and industrial sectors in developing time-efficient infrared thermography methods using drones [72]. Generally, a drone equipped with a thermal camera is operated remotely by a technician, capturing and saving images during the flight which are subsequently processed for the purpose of fault detection [72].
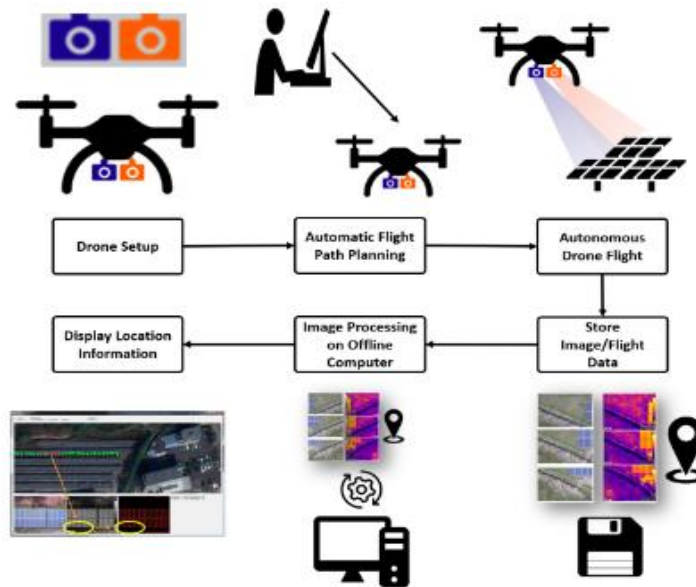
Figure 2.16: Infrared Thermography process [73].

The steps involved in this technique are as follows [72]:

➢ Set up the hardware structure of the drone, including the installation of the dual camera setup.

➢ Utilize a flight planning algorithm to automatically plan the path of the drone.

➢ The drone autonomously follows the designated path while capturing images, which are then saved to an SD card along with GPS information.

➢ Process the saved images using our proposed image processing algorithm on a desktop computer.

➢ Display the locations of the defective solar panels to the user.

Example: An experiment was developed in four scenarios: at 0° and 60° according to the horizontal plane of the PV panel, and 2 days at different temperatures [69].
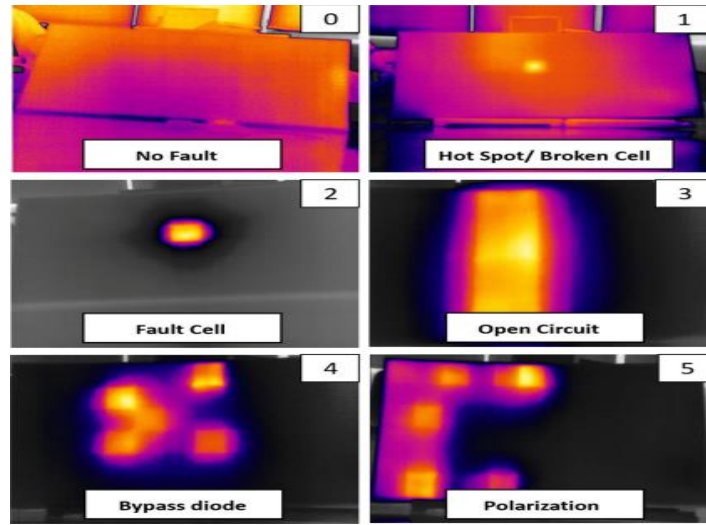
Figure 2.17: Faults detected by IRT experience [74].

The dataset of these experiments:

Exp0 T1 SI 131 (°C)	Exp0 T1 CWS (°C)	Exp0 T1 60° SI 131 (°C)	Exp0 T1 60° CWS (°C)	Exp1 T1 SI 131 (°C)	Exp1 T1 CWS (°C)	Exp1 T1 60° SI 131 (°C)	Exp1 T1 60° CWS (°C)	Exp2 T1 SI 131 (°C)	Exp2 T1 CWS (°C)	Exp2 T1 60° SI 131 (°C)	Exp2 T1 60° CWS (°C)
22.17	24.14	22.18	24.2	22.66	24.67	22.34	24.54	26.33	28.38	26.33	28.38
22.27	24.15	22.05	24.2	22.56	24.65	22.48	24.53	26.24	28.31	26.24	28.31
21.15	24.15	21.92	24.21	22.84	24.66	22.45	24.52	26.33	28.28	26.33	28.28
22.64	24.27	21.97	24.21	22.72	24.65	22.29	24.51	25.93	28.29	25.93	28.29
21.40	24.15	22.24	24.22	22.86	24.67	22.55	24.52	25.75	28.17	25.75	28.17
21.23	24.1	22.14	24.21	23.23	24.65	22.50	24.53	26.36	28.28	26.36	28.28
21.79	24.14	22.09	24.23	22.85	24.66	22.55	24.52	25.83	28.35	25.83	28.35
21.53	24.16	22.24	24.21	22.75	24.64	22.51	24.53	26.48	28.27	26.48	28.27
21.83	24.12	21.99	24.19	22.77	24.63	22.28	24.51	26.47	28.33	26.47	28.33
22.40	24.14	22.27	24.16	22.81	24.61	22.44	24.51	25.79	28.35	25.79	28.35
21.53	24.16	22.20	24.15	22.83	24.65	22.59	24.52	25.86	28.27	25.86	28.27
22.39	24.17	22.19	24.17	23.40	24.59	22.37	24.53	26.81	28.26	26.81	28.26
21.84	24.14	22.14	24.17	22.77	24.58	22.43	24.51	26.77	28.21	26.77	28.21
21.63	24.15	22.10	24.18	22.58	24.58	22.61	24.52	25.86	28.09	25.86	28.09
21.52	24.21	22.21	24.18	22.87	24.58	22.66	24.50	25.81	28.31	25.81	28.31
17.99	20.81	17.41	19.96	18.97	21.36	19.94	21.77	23.60	24.89	25.43	26.15
18.39	20.82	17.60	19.96	19.27	21.38	20.00	22.79	23.84	24.72	25.79	26.42
18.37	20.84	17.57	19.98	19.22	21.36	20.22	23.02	23.09	24.79	25.65	26.38
18.49	20.81	17.69	20.05	19.16	21.35	19.83	22.99	23.67	24.79	25.54	26.39
18.40	20.81	17.75	20.02	19.13	21.34	20.03	22.97	23.28	24.82	25.92	26.42
18.40	20.84	17.83	20.03	19.11	21.36	20.17	23.00	23.43	24.84	25.64	26.35
18.40	20.85	17.71	20.04	19.17	21.36	19.90	23.02	23.21	24.77	25.69	26.38
18.58	20.85	17.81	20.06	19.16	21.33	19.91	23.06	23.55	24.78	26.14	26.07
18.43	20.86	17.59	20.06	19.18	21.35	20.21	23.07	23.57	24.84	25.39	26.49
18.46	20.87	17.72	20.07	19.47	21.34	20.14	23.09	23.20	24.82	25.83	26.28
18.37	20.89	17.71	20.08	19.19	21.35	20.21	23.11	23.56	24.73	25.90	26.43
18.46	20.89	17.71	20.09	19.19	21.33	20.17	23.12	23.43	24.83	25.56	26.19
18.36	20.9	17.85	20.13	19.18	21.32	20.77	23.14	24.11	24.8	25.70	26.39
18.37	20.91	17.82	20.13	19.16	21.31	20.47	23.13	22.92	24.86	26.04	26.4
18.35	20.93	17.71	20.12	19.28	21.31	20.39	23.13	23.24	24.85	25.98	26.28

Figure 2.18: Dataset of the previous IRT experience [61].

4.2   Image processing techniques:

The objective of Digital Image Processing (DIP) is to extract meaningful information from images, detect patterns, and identify objects [70]. It can be processed from different types of imaging as explained before.

 A digital image is composed of a finite number of elements called pixels, each with a unique location and intensity [70]. DIP techniques employ various operations on these pixels to transform the images, enabling automated interpretation by systems or machines [70].

4.2.1 Segmentation by using RGB camera:

As a first step in detecting defects in the photovoltaic module, it is needed to segment it [75]. For applying this method, we have stages to respect starting with pre-processing, image thresholding, and noise reduction to connected components analysis and then we get segmented module.

The process involving a reduction in variables to describe and understand large volumes of data is termed feature extraction [76]. Before feature extraction, the acquired PV Module's aerial images were resized to a uniform size of 512×512 pixels [76]. Additionally, the color space of the images is converted into grayscale and provided as input of size $512 \times 512 \times 1$ for the application of segmentation techniques [76].

The image is represented as a function I, which maps the pixel positions (i, j, c) to intensity values in the range [0, 1]. The image can have either one or three channels (c = 1 or c = 3), with the latter representing a color image in the RGB space. The RGB channels are denoted as Ir, Ig, and Ib, corresponding to red, green, and blue channels, respectively. To segment a photovoltaic module from the background, a color space change is applied, converting the image into a grayscale denoted as G. The conversion formula for grayscale is given. In the next step, the image is thresholder to separate the PV modules from the background. The resulting binary image B is determined by comparing the threshold value (th) to the modified grayscale image G*. If G*(i, j) is less than the threshold, B (i, j) is set to 0; otherwise, it is set to 1 [75].

After this process, the result is a black-and-white mask, that has the lighter pixels of the original image as 1 and the darker as 0 [77]. The binary image also passes through a hole-filling process, when possible, holes are excluded, making the image clearer [77].

Morphological operators as dilatation and opening are applied in order to filter the segments and obtain only the segments of interest, then the final mask will have the pixels corresponding to the faults in the original image as 1 and the rest of the pixels as 0 [77].
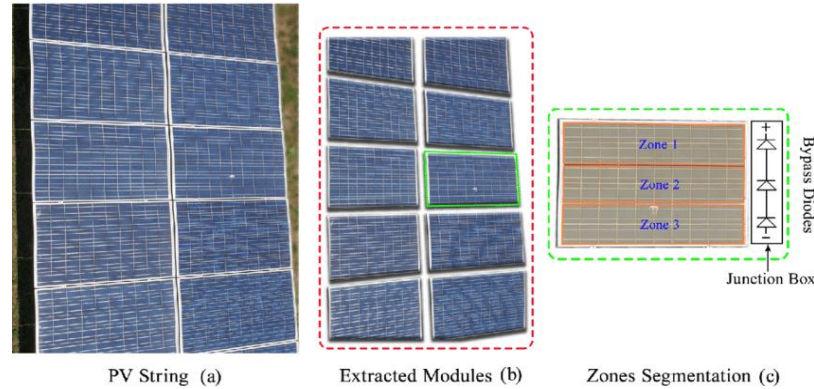
Figure 2.19: Segmentation of PV array by RGB camera [78].

4.2.2 **The Convolutional Neural Network (CNN) using Thermal imaging camera:**

The most popular of these techniques in image processing is by using Deep Learning, such as the Neural Network especially convolutional neural networks in the photovoltaic field.

These sequences consist of layers, each with a distinct role in transmitting the input signal where there are three main types of neural layers: (i) convolutional layers (ii) pooling layers and (iii) fully connected layers [70]
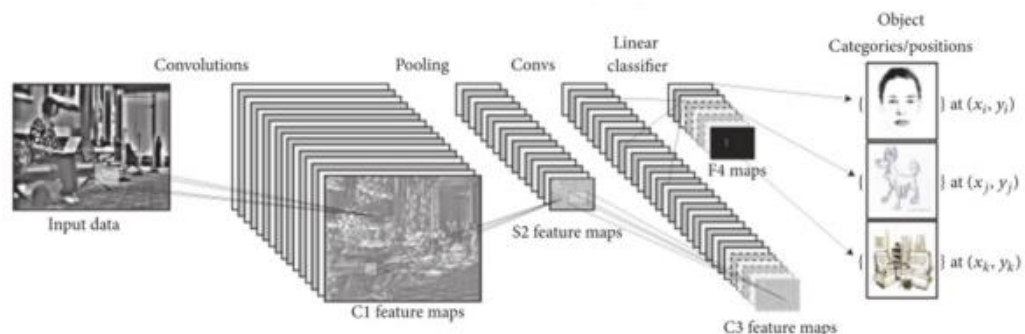
Figure 2.20: CNN architecture [79].

The proposed approach comprises four key steps: obtaining AIRT images, employing DIP techniques for image analysis, generating a dataset, and using CNN for classification and failure detection [77].

1. **The acquisition of aIRT images:** it requires the PV modules images taken by a handled thermal camera or by thermal images captured using unmanned aerial vehicles (aIRT)

2. **The application DIP techniques for image analytics:** before moving to the detection, the image processing; such as the segmentation is the first procedure that facilitates CNN technique.

3. **The creation of dataset:** This showcases data augmentation, which is a method to enhance the variety of your training dataset by applying random yet realistic transformations, like image rotation [80].

4. **The classification/failure detection by the CNN:** To automate classification in the domain of Foreground Segmentation, the process involves fine-tuning a pre-trained model using Keras and TensorFlow [77]. With these skills, you will be equipped to train your own Convolutional Neural Networks model and effectively tackle real-world problems [81].

5.   CONCLUSION:

As a consequence of human errors; it is suggested to introduce unmanned aerial vehicle (UAV) technology in photovoltaic systems in each of the visual, thermal imaging, and electroluminescence imaging integrating with sensors depending on the type of photography used. This will be very useful in efficient time management of inspection and cost reduction.

By explaining these methods for detecting faults, it became clear that they are all effective and practical in this matter. However, in comparison with each other and to choose the best among them (from results of Table II-1). It is noticed that they are somewhat uneven according to the type of fault, where the segmentation technique appears very similar to visual inspection, and the methods of measuring characteristics such as PV instruments and weather stations are very effective in electrical and thermal defects. While artificial intelligence techniques combine visual, thermal, and electrical faults.

Chapter 3

Simulation of photovoltaic stations in the desert of Algeria

Chapter 3: Simulation of photovoltaic stations in the desert of Algeria

1. Introduction:

In this section, we present the basics of the study we made to have a better knowledge of the inspection area by simulating the desired system.

We utilized the PVsyst software that we learned to operate during a training session at SOUNDOUS Energy Group in Boumerdès, Algeria. We conducted two simulations of a photovoltaic station, one for TAMANRASSET and another for ADRAR, using modules with similar characteristics to achieve a power output of 13 MW under two distinct weather conditions.

Our explanation will focus on the variations in operating conditions that can maximize the amount of solar irradiation, resulting in increased power output from the solar panels, including current and voltage. Additionally, we will identify the factors that can negatively impact the performance of the panels, leading to reduced yield.

2.   PVsyst software:

With a global user base spanning thousands of engineers, PVsyst Software is a comprehensive solar design tool that has become the industry standard for large and utility-scale solar installations [82].

This figure represents the logo of the PV system.

Figure 3.1 : PVsyst's logo [82].

With PVsyst, users can input detailed information about their solar systems, such as data on the solar PV modules and inverters, allowing for a comprehensive simulation of the system's performance under different conditions [83]. It is advanced features and capabilities make it easier to design grid-connected PV systems with precision and accuracy [82].

The interface of PVsyst software

This figure represents the interface of the software:
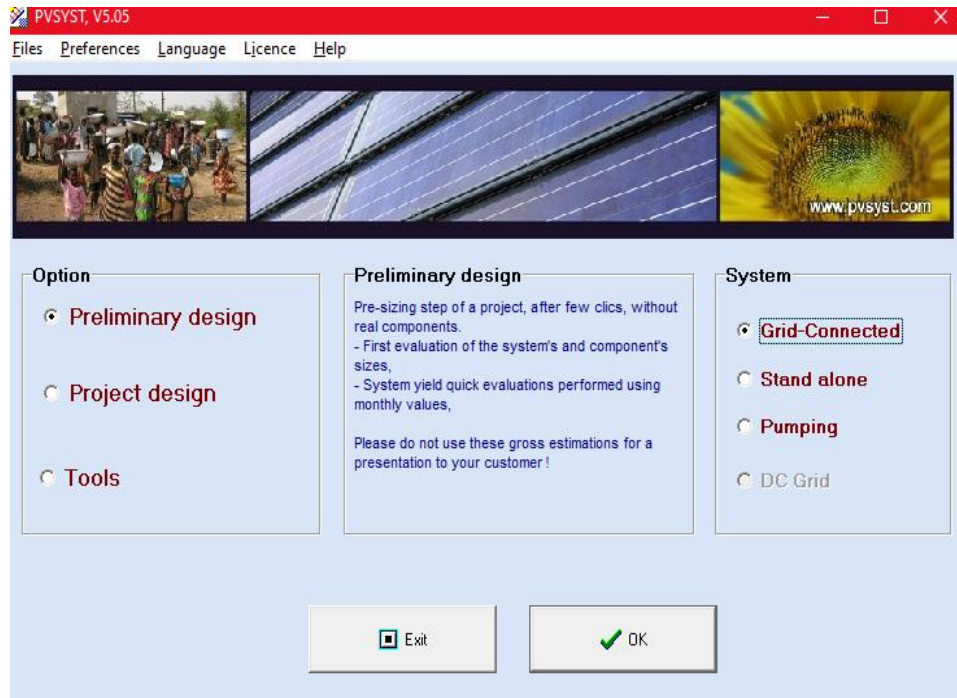
Figure 3.2: The interface of PVsyst software.

3.   Simulation of Tamanrasset and Adrar photovoltaic stations:

To simulate a ground, certain features need to be defined, including geographical site parameters, the desired power output in Megawatts, the quantity and dimensions of the panels, the number of strings, the type of modules, the number and type of inverters, and the installation method (whether in series, parallel, or a combination). Additionally, the azimuth, or the angle of the panels in relation to the sun's position, must also be taken into account.

We will explain the steps involved in using PV system introducing all the characteristics needed to install a photovoltaic station, as follows:

3.1   Horizon definition:
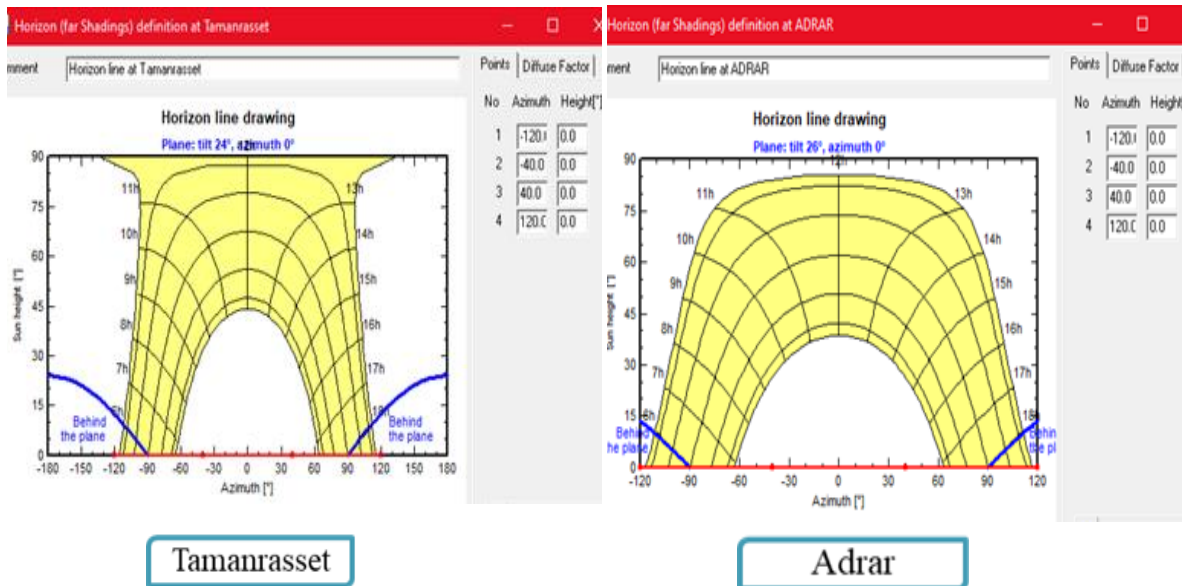
Figure 3.3 : The horizon definition.

The horizon definition graph shows the angle of the horizon at a specific location and time of day. The graph is important for designing solar panel installations as it helps to identify the optimal orientation and tilt angle for solar panels to maximize energy generation.

Where in this case, we see that in Tamanarasset the angle of the sun reaches the overhead 90° quickly, starting at 11 a.m. However, in Adrar we noticed that the sun moves gradually to the maximum which is approximately 83°.

3.2   Geographical coordinates:

The Geographical site parameters table is one of the most important tables in PVsyst software. It is used to input the geographical location data of the site where the photovoltaic (PV) system is installed.

The table contains several parameters, including the latitude and longitude of the site, the time zone, altitude, and the local weather data. The latitude and longitude are essential parameters that determine the amount of solar radiation received at the site. The time zone is important for calculating the solar position throughout the day. The altitude is used to calculate the atmospheric conditions and the air mass.

The Geographical site parameters table can be filled manually as we did or imported from a database. We took the geographical locations as follows:

➢ Tamanrasset: 22°28'N 5°19'E (22.47, 5.31)

➢ Adrar: 27°54'N 0°19'E (27.90, 0.32)

It is important to ensure that the data entered in the table is accurate and up to date. Any errors in the data can lead to inaccurate simulation results, affecting the design and performance of the PV system.

Figure 3.4: Geographical coordinates of Tamanrasset.

Figure 3.5: Geographical coordinates of Adrar.

3.3   Geographic site parameters (monthly meteo):
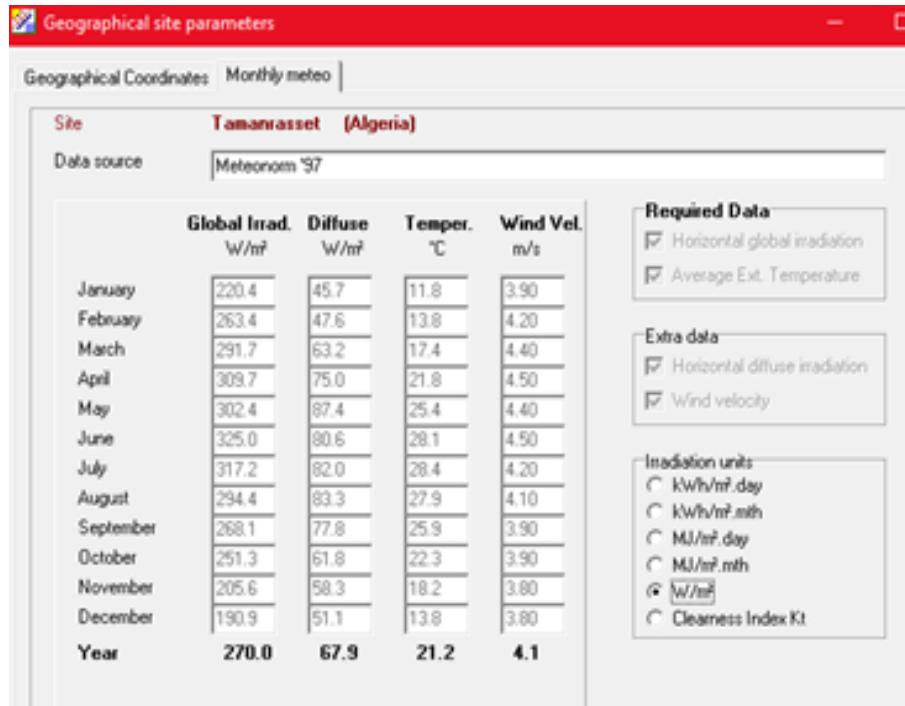
Figure 3.6: Geographical monthly meteo of Tamanrasset.
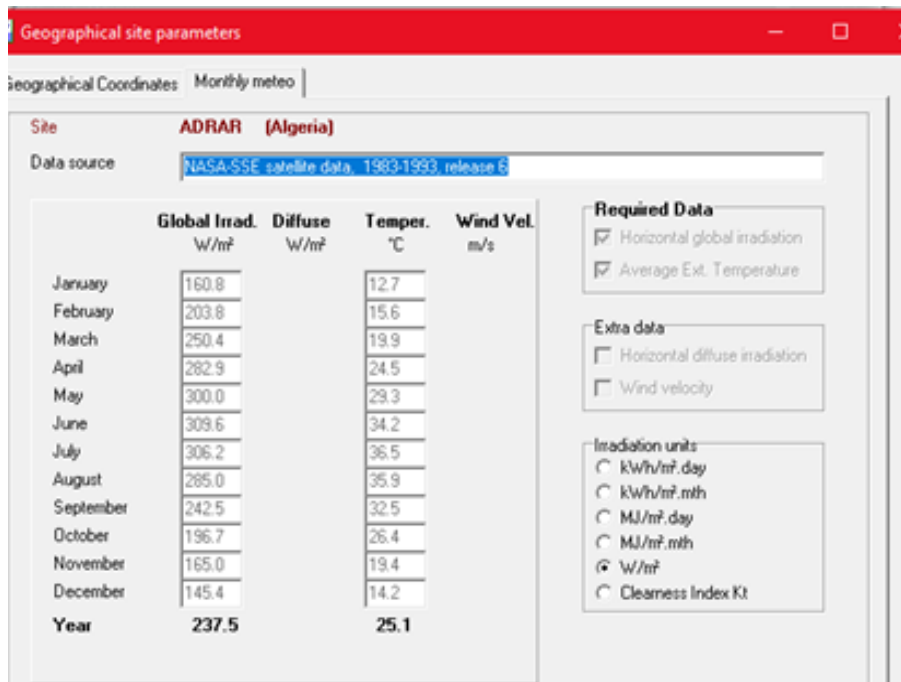
Figure 3.7: Geographical monthly meteo of Adrar.

The depicted figure provides information on the local weather data, which encompasses the ambient temperature, wind speed, and relative humidity. These parameters play a significant role in approximating the module temperature, which is a crucial factor in determining the efficacy of the PV system.

We can observe from the tables that both areas experience their highest global irradiation levels in the month of June. Moreover, Adrar is comparatively hotter than Tamanrasset in all months, but the irradiation levels show the opposite trend. Specifically, Tamanrasset consistently has higher irradiation levels than Adrar.

3.4   **Field parameter and orientation:**
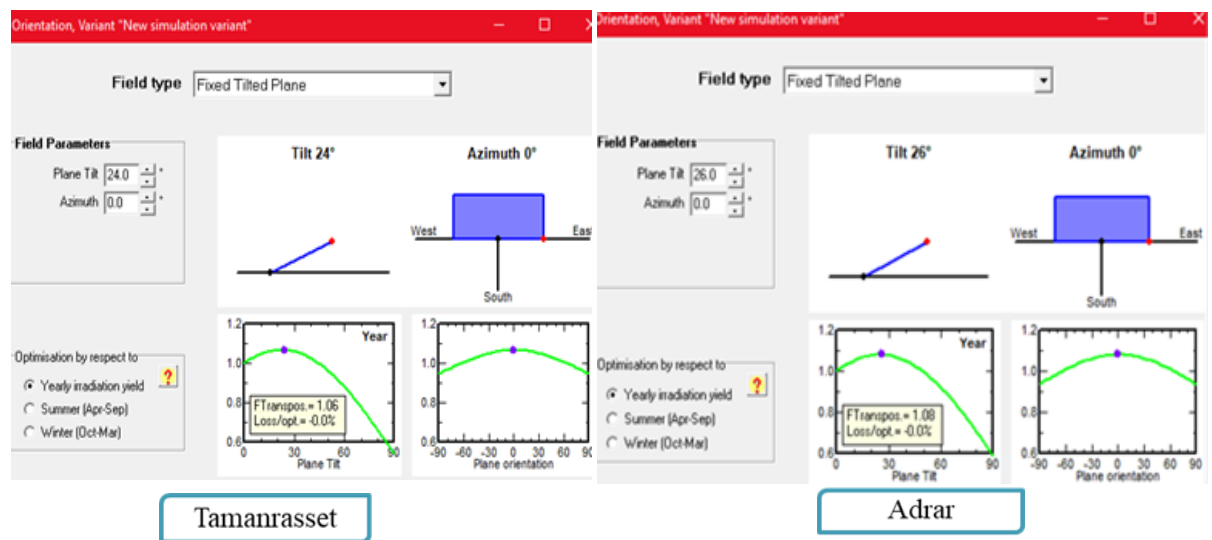
Figure 3.8: Orientation angle of panels (Azimuth).

Field parameter and orientation are important aspects of designing a photovoltaic (PV) system. Field parameter refers to the layout and arrangement of the PV modules, while orientation refers to the direction in which the modules are facing. These parameters can impact the performance of the PV system, as they affect the amount of solar irradiance that each module receives.

These graphs provide us with information regarding the optimal angle at which to attach the panels to our station in order to achieve maximum power output. Based on our analysis, we have determined that the optimal angle for the left graph is 24°, while for the right graph it is 26°, with the aim of minimizing any loss and achieving a 0.0% loss option. We can conclude that optimizing the field parameter and orientation of PV modules is significant in order to achieve maximum energy output and efficiency.

3.5   Photovoltaic characteristics:
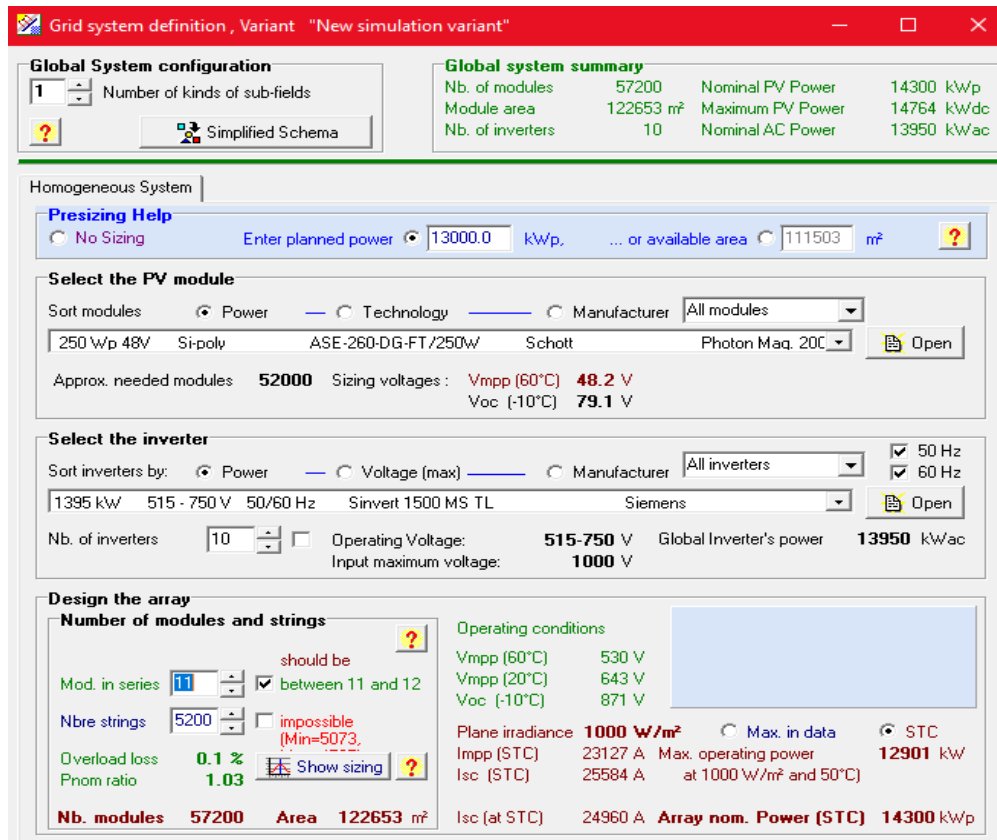
Figure 3.9: Grid system definition of both stations**.**

The grid system definition in PVsyst is a critical step in simulating solar energy systems. The "new simulation variant" feature allows users to create multiple simulations with different parameters. To define the Grid system in a new simulation variant, users input information about the grid, such as voltage, frequency, and short-circuit current. The simulation can then be run to analyze the system's behavior under different grid conditions, optimize performance, and ensure the system meets grid requirements.

Using the software formula, we have opted for a planned power output of 13000 kW, which will be achieved by installing 11 polycrystalline modules, each with a capacity of 250 W, connected in series to form 5200 strings. Additionally, 10 inverters will be used in the setup. The software will also provide us with information regarding the surface area required for the installation.

3.6   Power of the PV module used

PV module: Schott, ASE-260-DG-FT/250W
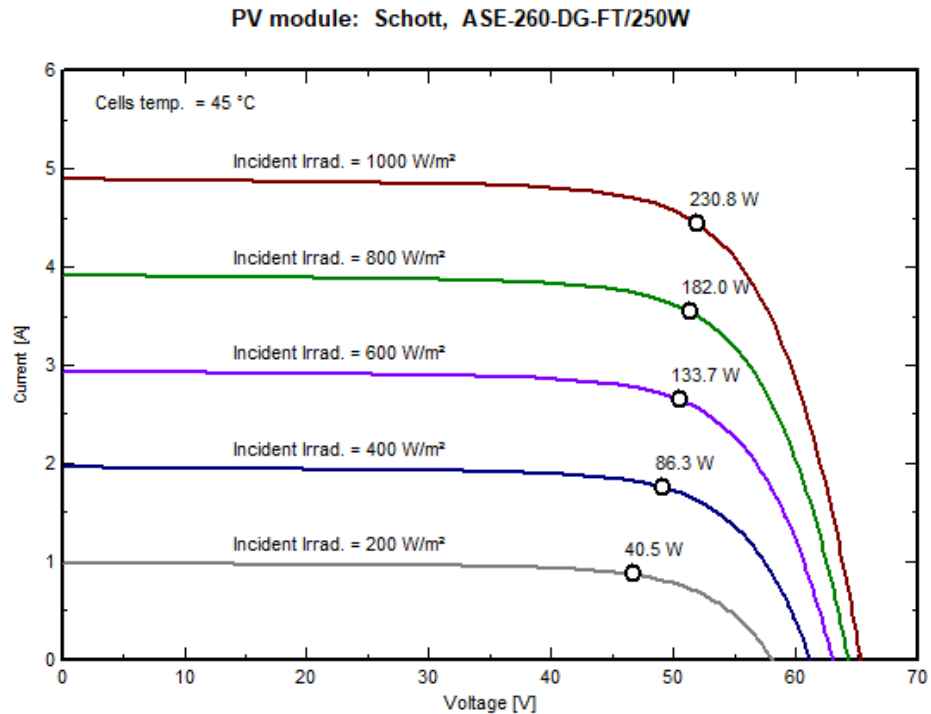
Figure 3.10: Graphs of power output according to the changes of incident irradiance .

The graph of the impacts of incident irradiance of the PV module's current and voltage is used to analyze the relationship between the amount of solar irradiance and the electrical output of a photovoltaic (PV) module. The x-axis represents the voltage of the module, while the y-axis represents the current generated by the module, where we observed that all the curves show a similar pattern of decreasing.

It shows us the effect of changing levels of incident irradiance on the electrical output of the PV module. At low levels of irradiance, the module produces a low electrical output, while at high levels of irradiance, the module produces a higher electrical output. The graph can help us to optimize the performance of the PV system by identifying the optimal levels of irradiance at which the system can generate the maximum amount of power.

The graph also shows the maximum power point (MPP) of the PV module, which is the point at which the module generates the most power. The MPP is important because it represents the optimal operating conditions for the module and can be used to optimize the design and performance of the PV system.

3.7   General Schema and Wiring:
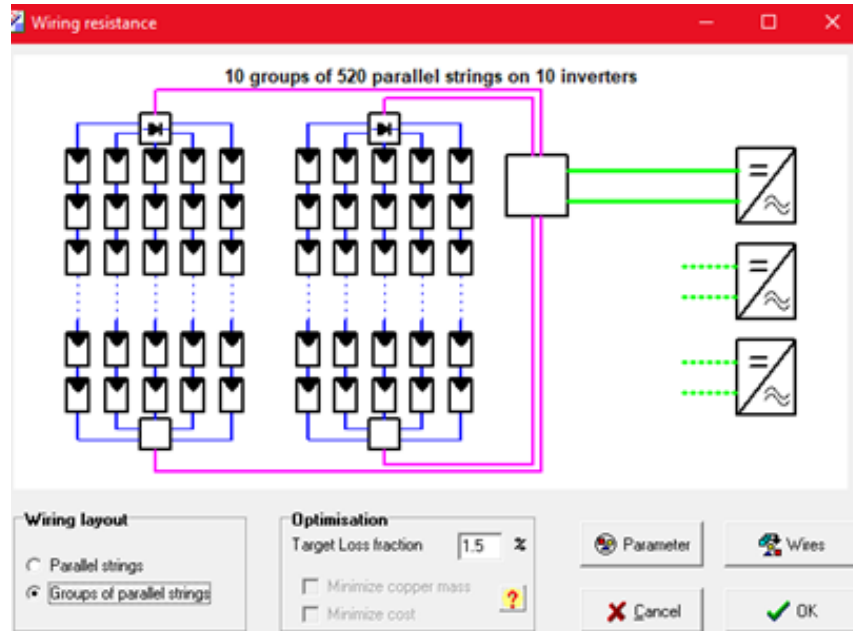
Figure 3.11: Installation of the Photovoltaic stations.

The General Schema and Wiring feature are a valuable tool for designing and optimizing the electrical components of a photovoltaic system. By creating a detailed schematic of the system and simulating its electrical performance.

We made a general Schema and Wiring to create a graphical representation of the electrical connections in a photovoltaic (PV) system. This feature is important for designing and optimizing the electrical components of a PV system, such as inverters, batteries, and charge controllers. In which, it divided us the station into 10 groups of 520 parallel strings on 10 inverters.
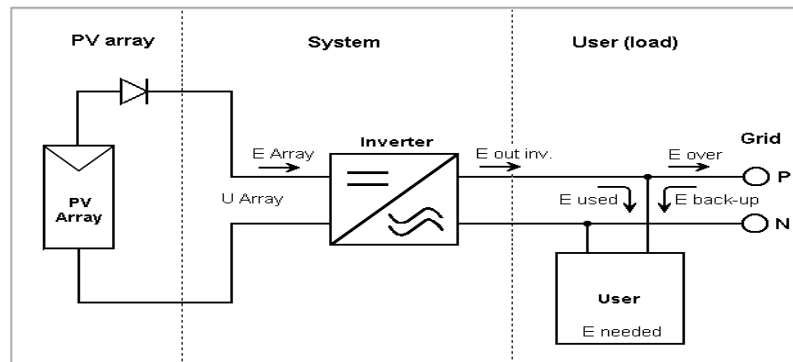
Figure 3.12: Electrical circuit of one photovoltaic array.

The General Schema and Wiring feature offered us to specify the electrical characteristics of each component in the system, such as voltage, current, and power ratings as in the schema. This information is used to calculate the electrical losses in the system and to optimize the system's performance.

Advantages of the General Schema and Wiring:

➢ It allows users to simulate the electrical performance of the system under different conditions. For example, users can simulate the performance of the system under different levels of solar irradiance or under different battery charging and discharging conditions.

➢ Permits to identify potential issues with the system's electrical design before the system is installed. By simulating the electrical performance of the system, users can identify areas of high electrical losses or other issues that may impact the system's performance.

3.8   Array and inverter sizing conditions (AC energy kWh/):
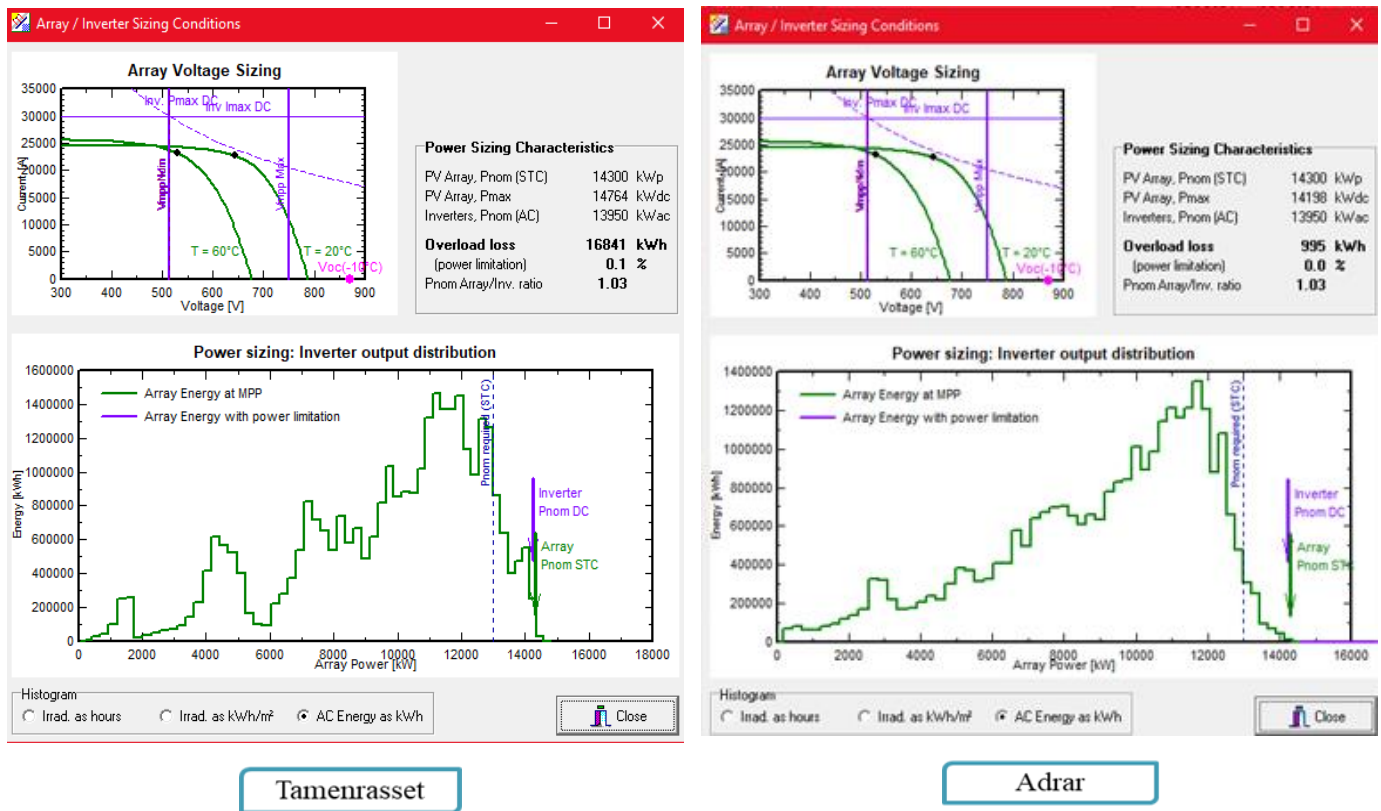
Figure 3.13: Graphs of array voltage and inverters sizing.

These figures help us to contextualize the consequences of the array size that we chose. The first one on top shows the noted graph which represents the voltage constraints that determine the number of modules that can be connected in series. It includes the PV array I-V curves represented with green graphs which corresponding to an irradiance of 1000 W/m². The curve shifted to higher voltages represents winter conditions when operating around 20°C, the second one is shifted to lower voltages represents summer conditions at 60°C. the open circuit voltage (Voc) at the lowest possible temperature is also shown and defined as -10°C.

The vertical purple graph shows the lower and higher operating voltage limits of the inverter.

The Power Sizing of Inverter Output graph is used to determine the optimal power output of the inverter. This graph shows the relationship between the inverter power output and the AC energy output in kWh per year. The x-axis of the graph represents the inverter power output in kW, and the y-axis represents the AC energy output in kWh per year. The graph also shows the efficiency of the inverter at different power outputs under different weather conditions.

We observed that the array energy at MPP in the Adrar station is growing exponentially and decreased rapidly until it disappeared completely, whereas in the other station, it is being enhanced in an oscillating manner and then decreased gradually.

The loss is displayed above the power characteristics, by default PVsyst sets an overload loss limit of 3%. If the overload are between 0.1% and 0.3%, the system considers the inverter to be slightly undersized and displays an orange warning. In this case, PVsyst still allow you to run the simulation. Else, it gives you an error message in red, and the simulation is not possible.

Both graphs help in determining the optimal voltage and power output of the PV system to maximize the energy output while considering factors such as shading, temperature, and weather conditions. By analyzing these graphs, users can make informed decisions about the PV system design and ensure that the system is efficient and cost-effective.

It is important to note that these graphs are interdependent and should be analyzed together to achieve the optimal PV system design. The Array Voltage Sizing graph affects the Power Sizing of Inverter Output graph, and vice versa. The optimal system design should balance the array voltage and inverter power output to achieve the highest energy output and efficiency.

4.   THE OBTAINED RESULTS:

4.1   Loss diagram during a year:

Loss diagram for "New simulation variant" - year

2365 kWh/m²   Horizontal global irradiation
                                    +6.6%   Global incident in coll. plane
                                    -2.9%   IAM factor on global
2448 kWh/m² * 122653 m² coll.   Effective irradiance on collectors
efficiency at STC = 11.7%   PV conversion
35182388 kWh   **Array nominal energy (at STC effic.)**

                                    -16.4%   Array Losses (Temp, Mod. Qual., Mism., Res.)

29409718 kWh   **Array virtual energy at MPP**

                                    -1.9%   Global inverter losses
28844306 kWh   **Available Energy at Inverter Output**
28844306 kWh   **Energy injected into grid**

TAMANRASSET

Figure 3.14: Loss diagram during a year.

Loss diagram for "New simulation variant" - year

2081 kWh/m²   Horizontal global irradiation
                                    +7.8%   Global incident in coll. plane
                                    -2.9%   IAM factor on global
2178 kWh/m² * 122653 m² coll.   Effective irradiance on collectors
efficiency at STC = 11.7%   PV conversion
31295536 kWh   **Array nominal energy (at STC effic.)**

                                    -17.9%   Array Losses (Temp, Mod. Qual., Mism., Res.)

25679780 kWh   **Array virtual energy at MPP**

                                    -2.1%   Global inverter losses
25143036 kWh   **Available Energy at Inverter Output**
25143036 kWh   **Energy injected into grid**

ADRAR

Figure 3.15: Loss diagram during a year.

These diagrams represent the overload losses in the year which is significant output of any PVsyst simulation.

We noticed that the losses of each array nominal energy and array virtual energy at MPP in Adrar station are more than those in Tamnarasset with 1.5% and 0.2% respectively. The same thing with the horizontal global irradiation where in Adrar are +7.8% and in the second area are +6.6%.

By analyzing the array losses and horizontal irradiation losses in the loss diagram, it is possible to identify the factors that are causing energy loss in the system and take corrective action. For example, if the array losses are high, it may indicate that the solar panels need to be repositioned or the shading needs to be reduced. If the horizontal irradiation losses are high, it may suggest that the orientation of the panels needs to be adjusted to face the sun more directly.
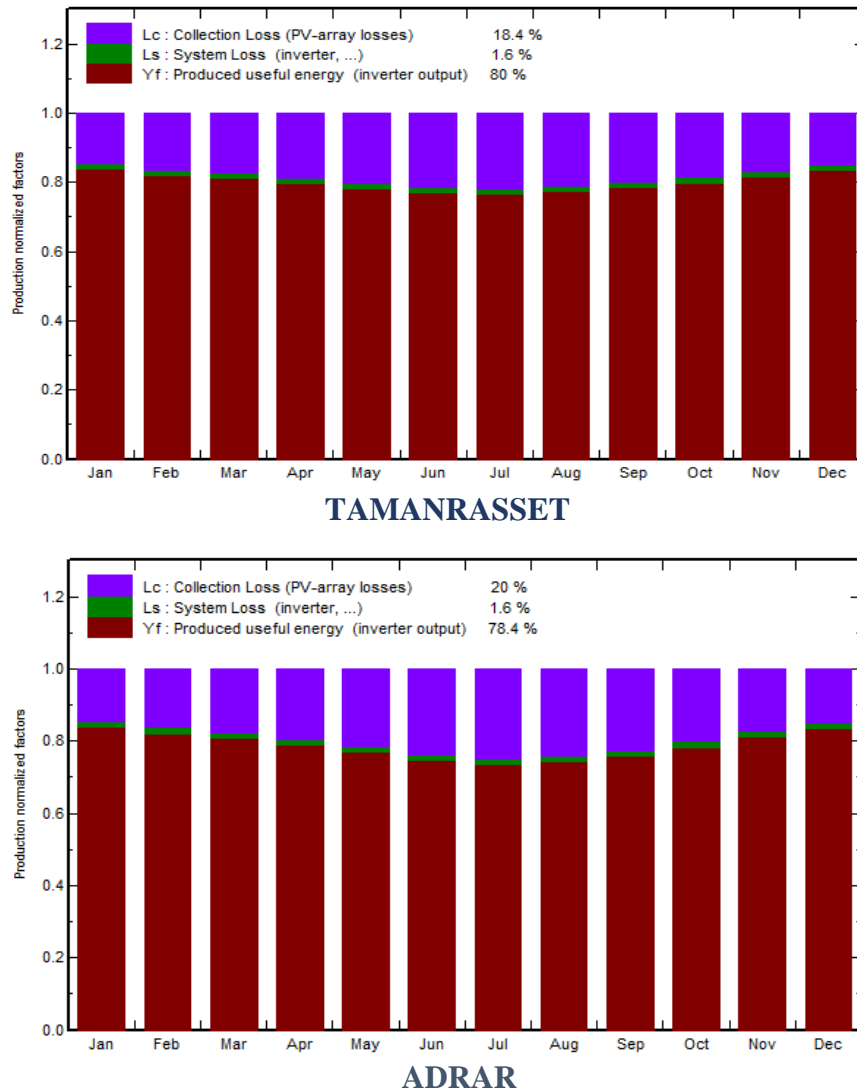
Figure 3.16: Graphic columns of useful energy and losses.

4.2   Normalized production and loss factors:

The Monthly Normalized Production column shows the percentage of energy produced by the system for each month, included the useful energy output, the collection and the system losses for that month. This column helps identify any seasonal variations in the system's performance due to factors such as changes in the PV array, inverters losses... etc.

We noticed from the two graphic columns that PV array losses in Adrar station are more than in Tamanrasset with 1.6% which reduces the generated energy that can be stored for later use.

The Monthly loss Factors column provides a breakdown of the different factors contributing to energy loss for each month, which helps identify any seasonal variations in the factors that are impacting the system's performance. By analyzing these columns, you can identify any seasonal trends in the system's performance and adjust the system accordingly to optimize energy production throughout the year. Overall, the monthly versions of these graphic columns in PVsyst software provide valuable insights into the monthly performance of a PV system and help identify areas for improvement to maximize energy production throughout the year.

4.3   Partial shadings on one cell:
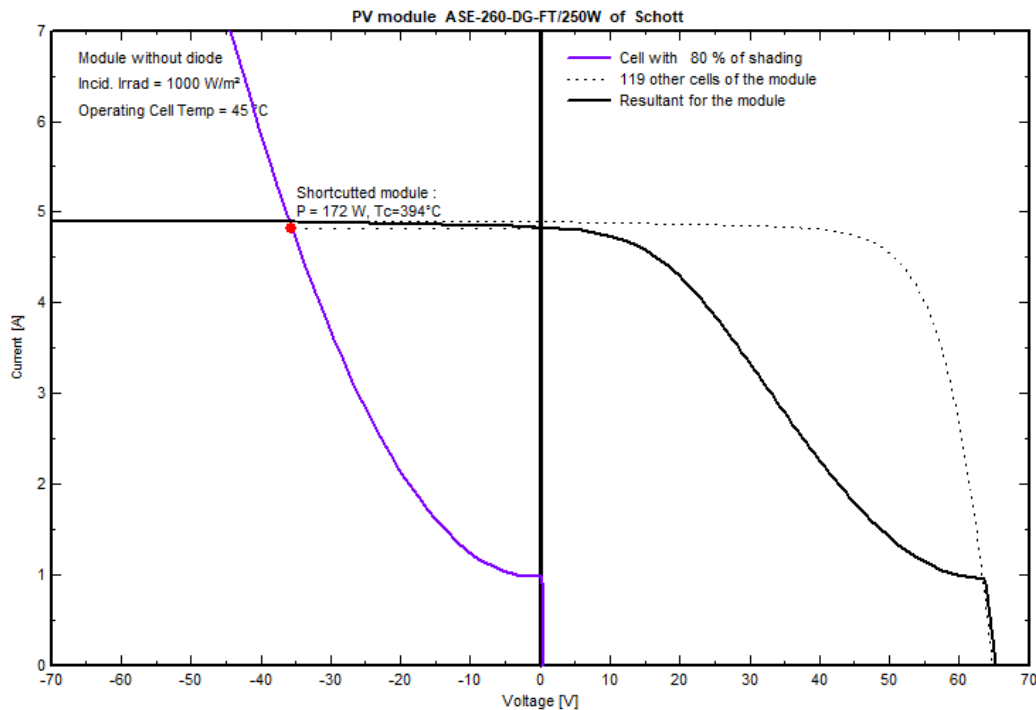
Figure 3.17: Graph indicates partial shadings on one cell.

The graphs show the voltage and current output of 120 cells within a module, where this last is without diodes and under 1000 W/m2 of irradiation also the operating cell temperature is 45° C. The x-axis represents the voltage

output, and the y-axis represents the current output. The shaded area in the graph represents the range of voltages and currents that the cell can operate under.

The graph in purple illustrates the voltage and current output of a cell that is 80% shaded. On the other hand, the dotted graph shows the anticipated output of the other 119 cells in the module. The last graph is a

combination of both the purple and dotted graphs, reflecting the overall outcome of the shading effect on the module's performance. The outcome indicates that the graph can be utilized to enhance the PV system's design and comprehend the impact of shading on its efficiency.

5.   CONCLUSION:

The power energy output of solar modules is directly influenced by environmental factors such as temperature and irradiance. Temperature affects the performance of solar panels by increasing the resistance of the materials used in the solar cells. This results in a decrease in the power output of the panels. On the other hand, irradiance refers to the amount of solar radiation that reaches the solar panel. The more sunlight the panel receives; the more energy it can produce.

Interestingly, temperature and irradiance are not directly related to each other. This means that it is possible to have high levels of irradiance with low temperatures or vice versa. This was demonstrated by the two stations in Tamanrasset and Adrar, where Tamanrasset had a low temperature but a very bright radiation level throughout the year, while Adrar had the opposite.

To further understand the impact of these factors on power energy output, we used software to evaluate the effect of irradiance and shading on photovoltaic panels. Our analysis revealed that shading can significantly reduce the yield of power energy. This is because when a solar panel is shaded, the cells in the shaded area receive less sunlight, resulting in a decrease in the overall power output of the panel. Therefore, it is important to consider the impact of shading when installing solar panels to maximize their energy production.

PVsyst is a powerful software tool for designing, simulating, and analyzing photovoltaic (PV) solar energy systems. It offers a comprehensive suite of features for modeling the performance of PV systems, including detailed shading analysis, weather data importation, and financial analysis. This software is widely used in the solar energy industry and has a reputation for being accurate and reliable. While the software has a steep learning curve, it is well documented and supported by an active community of users. Overall, PVsyst is essential for anyone involved in the design, installation, or operation of PV solar energy systems.

The fourth chapter will talk about the simulation of the drone and its trajectory.

Chapter 4

Inspection and Detection System of Photovoltaic Faults by Drone

CHAPTER 4: Inspection and Detection System of Photovoltaic Faults by Drone

1. INTRODUCTION:

This study aims to design and simulate a control system for a drone to follow a desired trajectory accurately, capture images and process them to detect their faults. In this chapter, we describe the steps involved in the simulation of the drone control system using MATLAB/Simulink. We model the drone's motion equations using Newton's laws of motion, design and implement a control system to guide the drone along the desired trajectory, specify the waypoints for the drone's trajectory, generate a reference trajectory, and develop a controller that tracks the reference trajectory. We then simulate the model and analyze the simulation results to assess the drone's performance. After finishing with the drone's simulation, we move to the image processing part, describing the method, the dataset, and the program utilized step by step. We finally will show the results obtained from the program developed and discuss them.

2. CONCEPTION MODEL:

To have a general idea, we made a synoptic view of the global work carried out in the field of drone trajectory planning and inspection of the photovoltaic system by using image processing. It evolves into
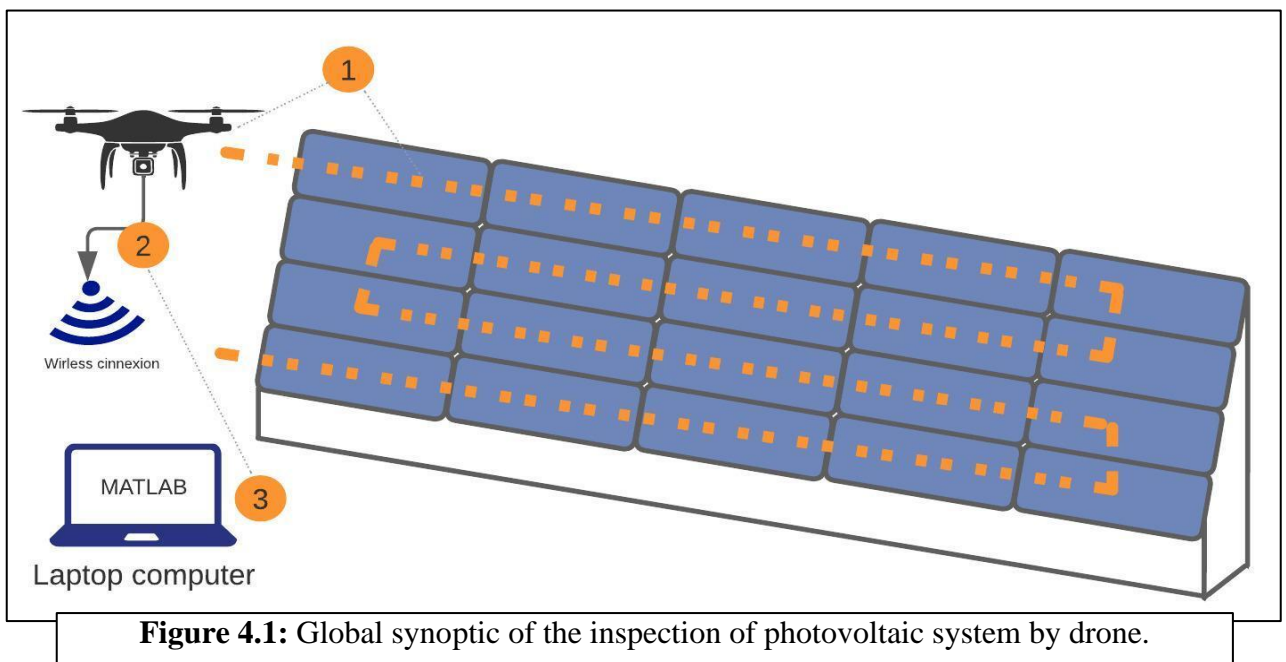
Figure 4.1: Global synoptic of the inspection of photovoltaic system by drone.

three steps which are:

> ➢ 1) Drone simulation, capturing images of the modules, and identifying their trajectory.
> ➢ 2) Sending the captured images to the computer via wireless connection.
> ➢ 3) Image processing to detect the photovoltaic module faults using MATLAB.

3.   SIMULATION OF THE DRONE AND ITS TRAJECTORY:

Before we get into the simulation of the drone and make it follow a certain trajectory, it is necessary to strike a balance between the mathematical model's theoretical aspects and the dynamic modeling's robustness.

To achieve this, certain compromises must be made. For example, it is assumed that the center of mass and the origin of the marker linked to the structure coincide. Additionally, the drone frame is assumed to be rigid and symmetrical, which results in the inertia matrix being assumed to be diagonal. To simplify the model, the effects of rotor vibration are neglected. Moreover, it is assumed that the lift and drag forces are proportional to the squares of the rotation speed of the rotors, which is an approximation that closely resembles the aerodynamic behavior of the system.

3.1   kinematics of the drone:

As we saw in chapter one, we will need two frames which are the inertial frame and the body frame, so before getting into the dynamic model of the drone we should define the rotation matrix:

In the field of aircraft flight dynamics, the orientation of the drone relative to the ground coordinate system is described using three Euler angles.

Using these Euler angles, a transformation matrix can be constructed to map the UAV coordinate system onto the ground coordinate system for each axis which is the following

$$Rx = \begin{bmatrix} 1 & 0 & 0 \\ 0 & \cos\varphi & \sin\varphi \\ 0 & \sin\varphi & \cos\varphi \end{bmatrix} \tag{4.1}$$

$$Ry = \begin{bmatrix} \cos\theta & 0 & \sin\theta \\ 0 & 1 & 0 \\ -\sin\theta & 0 & \cos\varphi \end{bmatrix} \tag{4.2}$$

$$Rz = \begin{bmatrix} \cos\psi & -\sin\psi & 0 \\ \sin\psi & \cos\psi & 0 \\ 0 & 0 & 1 \end{bmatrix} \tag{4.3}$$

The transformation matrix of drone coordinate system to ground coordinate system can be constructed as following:

$$R = RxRyRz = \begin{bmatrix} \cos\psi\cos\theta & \cos\psi\sin\theta\sin\varphi & \cos\psi\sin\theta\cos\varphi + \sin\psi\sin\varphi \\ \sin\psi\cos\theta & \sin\psi\sin\theta\sin\varphi & \sin\psi\sin\theta\cos\varphi - \cos\psi\sin\varphi \\ -\sin\theta & \cos\theta\sin\varphi & \cos\theta\cos\varphi \end{bmatrix} \tag{4.4}$$

3.2   Dynamic model of a quadcopter:

3.2.1 state variables:

in this simulation, we take 12 variables which are the position, velocity, and attitude of the body frame in the inertial frame, and angular rates.

$$\vec{x} = [X, Y, Z, \dot{X}, \dot{Y}, \dot{Z}, \varphi, \theta, \psi, p, q, r]^T \tag{4.5}$$

3.2.2 control variables:

We take four control inputs, which are total thrust, and moments of each control axis.

$$\vec{u} = [u_1, u_2, u_3, u_4]^T = [T_\Sigma, M_1, M_2, M_3]^T \tag{4.6}$$

3.2.3 Thrust and moment distributions:

Total thrust and moments generated by N number of rotors can be expressed as follows:

$$T_\Sigma = \sum_{i=1}^{N} T_i = k_T \sum_{i=1}^{N} \Omega_i^2 \tag{4.7}$$

$$M_1 = -\sum_{i=1}^{N} l_i \sin(\xi_i) T_i = -k_T \sum_{i=1}^{N} l_i \sin(\xi_i) \Omega_i^2 \tag{4.8}$$

$$M_2 = \sum_{i=1}^{N} l_i \cos(\xi_i) T_i = -k_T \sum_{i=1}^{N} l_i \cos(\xi_i) \Omega_i^2 \tag{4.9}$$

$$M_3 = \sum_{i=1}^{N} O_i Q_i = k_Q \sum_{i=1}^{N} O_i \Omega_i^2 \tag{4.10}$$

Therefore, symmetric multi-copter with N = 4(quadcopter) and $l_i = l$ (same arm length), one can get the desired angular speed of each rotor by:

$$\begin{bmatrix} T_\Sigma \\ M_1 \\ M_2 \\ M_3 \end{bmatrix} = \begin{bmatrix} k_T & k_T & k_T & k_T \\ 0 & k_T{}^l & 0 & -k_T{}^l \\ k_T{}^l & 0 & -k_T{}^l & 0 \\ k_Q & -k_Q & k_Q & -k_Q \end{bmatrix} \begin{bmatrix} \Omega_1^2 \\ \Omega_2^2 \\ \Omega_3^2 \\ \Omega_4^2 \end{bmatrix} \tag{4.11}$$

$$\begin{bmatrix} \Omega_1^2 \\ \Omega_2^2 \\ \Omega_3^2 \\ \Omega_4^2 \end{bmatrix} = \begin{bmatrix} k_T & k_T & k_T & k_T \\ 0 & k_T{}^l & 0 & -k_T{}^l \\ k_T{}^l & 0 & -k_T{}^l & 0 \\ k_Q & -k_Q & k_Q & -k_Q \end{bmatrix}^{-1} \begin{bmatrix} T_\Sigma \\ M_1 \\ M_2 \\ M_3 \end{bmatrix} \tag{4.12}$$

Or thrust required as follows:

$$\begin{bmatrix} T_\Sigma \\ M_1 \\ M_2 \\ M_3 \end{bmatrix} = \begin{bmatrix} 1 & 1 & 1 & 1 \\ 0 & l & 0 & -l \\ l & 0 & -l & 0 \\ k_Q/k_T & -k_Q/k_T & k_Q/k_T & -k_Q/k_T \end{bmatrix}^{-1} \begin{bmatrix} T_1 \\ T_2 \\ T_3 \\ T_4 \end{bmatrix} \tag{4.13}$$

3.2.4 equations of motion:

In total we have 12 state variables that are divided into two groups, 6 state variables of a translational motion $(\dot{X}, \dot{Y}, \dot{Z}, \ddot{X}, \ddot{Y}, \ddot{Z})$, and 6 other state variables that represents the rotational motion $(\dot{\varphi}, \dot{\theta}, \dot{\psi}, \dot{p}, \dot{q}, \dot{r})$.

3.2.4.1   Translational motion:

The rate of change for the 6 state variables from the beginning $(\dot{X}, \dot{Y}, \dot{Z}, \ddot{X}, \ddot{Y}, \ddot{Z})$ can be obtained by the following translational motion equations:

$$\dot{\vec{r}} = \vec{v}$$

$$m\dot{\vec{v}} = mg\vec{a_3} + R \cdot T_\Sigma \cdot (-\vec{z}) \quad (Newton's\ 2nd\ law: \frac{d}{dt}(m\vec{v}) = \Sigma \vec{F_i}) \tag{4.14}$$

In detail:

$$\ddot{X} = -\frac{1}{m}(sin\,\psi \cdot sin\,\varphi + cos\,\psi \cdot sin\,\theta \cdot cos\,\varphi) \cdot T_\Sigma \tag{4.15}$$

$$\ddot{Y} = -\frac{1}{m}(-cos\,\psi \cdot sin\,\varphi + sin\,\psi \cdot sin\,\theta \cdot cos\,\varphi) \cdot T_\Sigma \tag{4.16}$$

$$\ddot{Z} = -\frac{1}{m}cos\,\theta \cdot cos\,\varphi \cdot T_\Sigma + g \tag{4.17}$$

3.2.4.2   Rotational motion:

The rate of change for the other 6 state variables behind $(\dot{\varphi}, \dot{\theta}, \dot{\psi}, \dot{p}, \dot{q}, \dot{r})$ can be obtained from the following motion equations:

$$\dot{R} = R \cdot sk(\vec{\omega}) \tag{4.18}$$

$$I\dot{\vec{\omega}} = -\,\vec{\omega} \times I\vec{\omega} + M \;(Newton's2nd\;law: \frac{d}{dt}(\vec{H}) = \sum \vec{M_i}) \tag{4.19}$$

Using Euler angles;

$$\begin{pmatrix} \dot{\varphi} \\ \dot{\theta} \\ \dot{\psi} \end{pmatrix} = \begin{bmatrix} 1 & \sin\varphi\,\tan\varphi & \cos\varphi\,\tan\theta \\ 0 & \cos\varphi & -\sin\varphi \\ 0 & \sin\varphi\,\sec\theta & \cos\varphi\,\sec\theta \end{bmatrix} \begin{pmatrix} p \\ q \\ r \end{pmatrix} \tag{4.20}$$

$$\dot{p} = \frac{I_{yy}-I_{zz}}{I_{xx}} \cdot qr + \frac{1}{I_{xx}} \cdot M_1 \tag{4.21}$$

$$\dot{q} = \frac{I_{zz}-I_{xx}}{I_{yy}} \cdot rp + \frac{1}{I_{yy}} \cdot M_2 \tag{4.22}$$

$$\dot{r} = \frac{I_{xx}-I_{yy}}{I_{zz}} \cdot pq + \frac{1}{I_{zz}} \cdot M_3 \tag{4.23}$$

3.3   Drone's trajectory:

Our work is focused on the photovoltaic system inspection via drone, so the drone should follow a specific trajectory to inspect the photovoltaic panels and detect all the surface. As we know, the photovoltaic panels are placed one next to another forming a string, and in photovoltaic centrals we can have a million of strings.
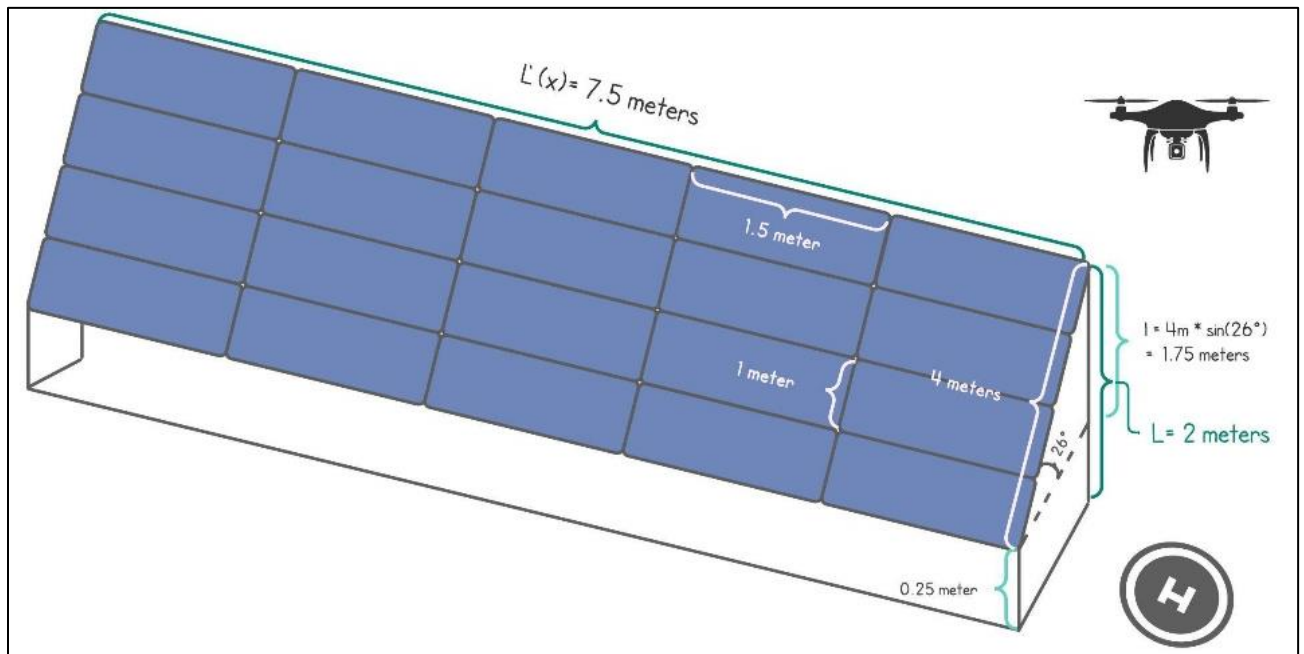
Figure 4.2: Photovoltaic string's dimensions.

To have a good perspective of the trajectory here is a drawing that shows the dimensions of the photovoltaic panels.

3.3.1 Experiment's conditions:

Taking the trajectory information into consideration, as the figure 1 shows, the height of the string is up to 2 meters, and in order to capture a good quality of images the drone should fly at a safe distance from the photovoltaic panels, for that we spaced the drone with 1 meter apart of the top panel so the drone is in an altitude of 3 meters from the ground. This altitude is maintained during the fly to reduce the risk of collision.

We chose a trajectory that almost looks like a square signal passing by the midline modules to inspect all their surfaces where the drone lands on the same side as the take-off point. In our project we took an example for only one array.
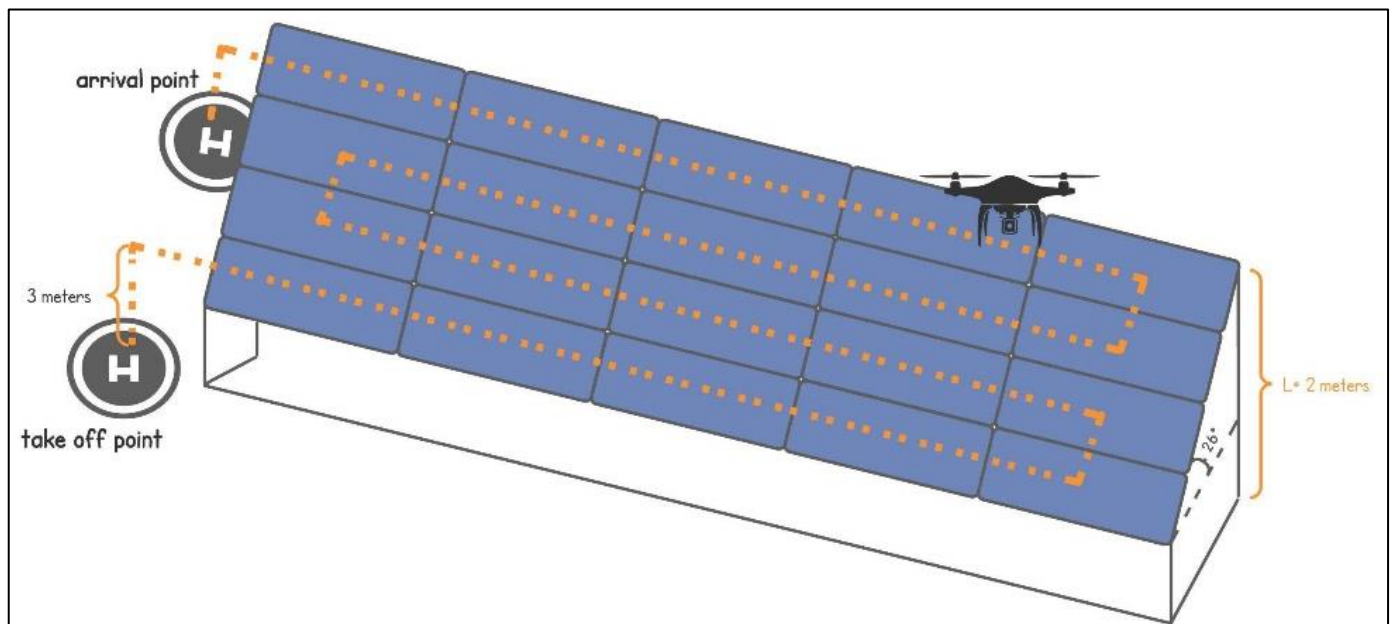
Figure 4.3: Drone's trajectory for photovoltaic inspection.

3.4   The choice of the simulation environment and the trajectory generation method:

In this simulation, we used MATLAB/Simulink, a programming platform that allows engineers and scientists to analyze and design systems, due to its ease of use and its powerful set of tools and a wide range of libraries that provide functionality for simulating a variety of systems, drones in our case, and functions

for numerical computation, data analysis, and visualization. In essence, MATLAB provides a comprehensive and robust environment for our work.

To generate the drone's trajectory, we noticed that the waypoint method is the most suitable one in this study. The waypoint method is an advanced navigation strategy employed in path planning and control. It consists of defining and incorporating intermediate reference points, known as waypoints, into the trajectory planning process. Waypoints serve as a signpost or a landmark along the desired path, enabling the system to effectively navigate complex environments while staying on the right path. This waypoint is a specific location or a point that has 3 geometric coordinates (a_x, a_y, a_z), this point is used as a reference point for navigation.

In fact, Photovoltaic central inspection involves examining a large area with photovoltaic arrays. By using the waypoint method, we can create a predetermined path that ensures complete coverage of the entire area, and a complete inspection of every panel, minimizing the chance of missing any potential issues.

3.5   Implementation of the program:

We have developed a program that enables a comprehensive visualization of the drone and its trajectory around the photovoltaic station. This program allows for a detailed and complete representation of the drone's movements and path.

Here are the detailed steps:

➢   Define the setup drone:

It is crucial to determine the physical characteristics of the drone like the mass(m), moment of inertia I (Ix, Iy, Iz), and the environment. In this simulation we are assuming a perfect environment (no wind disturbance or any kind of noise to shake the drone).

```
1    %% Setup Drone
2    m = 0.2 %the mass(kg)
3    I = [[0.1,0,0];[0,0.1,0];[0,0,0.08]] %Ix,Iy,Iz
4    % Environment
5    g = [0;0;-9.8]
```

Figure 4.4 : Drone's set up.

Set the drone's initial states position, Euler's angles, and body rate.

```
9     % Initial States
10    XYZ_0 = [1;2;0]         %drone's initial positions(x,y,z)
11    Euler_0 = [0;0;0]       %drone's initial Euler angles
12    body_rate_0 = [0;0;0] %drone's initial body rate
```

Figure 4.5 : Initial states of the drone.

Specifying the Euler rate function:

```
1     function [phi_d,theta_d,psi_d] = fcn(p,q,r,phi,theta,psi)
2         D = [[1 sin(phi)*tan(theta) cos(phi)*tan(theta)];
3               [0 cos(phi) -sin(phi)];
4               [0 sin(phi)/cos(theta) cos(phi)/cos(theta)]];
5         euler_rate = D*[p;q;r]
6         phi_d = euler_rate(1)
7         theta_d = euler_rate(2)
8         psi_d = euler_rate(3)
```

Figure 4.6 : Euler rate function.

➢ Set the waypoints:

We specify the location of each waypoint (x, y, z) according to the trajectory in figure 2, x represents the length of the array which is L' = 7.5 meters, y represents the distance between every midline of two modules, which is 1 meter, and as we explained before, the drone needs to have a safe distance between it and the photovoltaic array, for that z = 3 meters. To have a precise study we add the time between each waypoint.We store the coordinates of the waypoints in a matrix. Each row of the matrix represents a

WayPts ✕

⊞ 10x4 double

	1	2	3	4
1	0	0	0	1
2	0	0	3	5
3	7.5000	0	3	15
4	7.5000	1	3	25
5	0	1	3	35
6	0	2	3	40
7	7.5000	2	3	50
8	7.5000	3	3	55
9	0	3	3	65
10	0	3	0	70

Figure 4.7 : Waypoints array.

waypoint, the last value of each row determines the acquisition time. The columns correspond to the different coordinate dimensions and the acquisition time in seconds (x, y, z, time).

```
12   ⊟      for i = 1:length(WayPts)−2
13              dX(i) = (WayPts(i+2,1)−WayPts(i+1,1))/(WayPts(i+2,4)−WayPts(i+1,4))
14              dY(i) = (WayPts(i+2,2)−WayPts(i+1,2))/(WayPts(i+2,4)−WayPts(i+1,4))
15              dZ(i) = (WayPts(i+2,3)−WayPts(i+1,3))/(WayPts(i+2,4)−WayPts(i+1,4))
16          end
```

Figure 4.9 : Waypoints iteration loop.

Staying in the waypoints, we generated a program with the waypoints stored:

➢ Declaration and initialization of variables with empty arrays to store the derivative values of the waypoints.

```
24          x_sum = 0*t
25          z_sum = 0*t
26          y_sum = 0*t
27   ⊟      for k = 1:length(WayPts)
28              if k == 1 % time: 0−1 sec, 1st Waypts
29                  section = [0, WayPts(k,4)];
30                  start_section = section(1);
31                  end_section = section(2);
32
33   ⊞              for i = 1:length(z_sum) ⋯
40
41              elseif k == 2 % time: 1−5 sec, 2nd Waypts, take−off process
42                  section = [WayPts(k−1,4),WayPts(k,4)]
43                  start_section = section(1);
44                  end_section = section(2);
45
46   ⊞              for i = 1:length(z_sum) ⋯
```

Figure 4.10 : Trajectory generation loop.

➢ To calculate the derivatives of x, y, and z coordinates of the waypoints using limited differences, we generate a loop. It iterates over the waypoints and computes the difference in position divided by the difference in time (the 4th column of the waypoints matrix) and are then stored in the arrays we mentioned on top.

➢ To generates the trajectory, we create a loop that iterates over each waypoint in the waypoint's matrix. But before that we need 3 arrays that initialize with zeros and have the same length as t, while t goes from 0 to T final that represents the last acquisition time in the waypoint's array with a step of 0.1 seconds.

For k == 1, which the corresponds to the first waypoint, inside the loop that handles the time from 0 to the time value of the first waypoint in the matrix. It sets the values of the three arrays to zero during this interval of time.

For k == 2, which corresponds to the second waypoint which is the take-off point, inside the loop that

```
81          sigZ = [t;z_sum]
82          Zcmd = timeseries(sigZ(2:end,:),sigZ(1,:))
83          sigY = [t;y_sum]
84          Ycmd = timeseries(sigY(2:end,:),sigY(1,:))
85          sigX = [t;x_sum]
86          Xcmd = timeseries(sigX(2:end,:),sigX(1,:))
```

Figure 4.11 : command variables generation.

handles the gap between the two instants of the first and second waypoints. It sets the arrays this time to
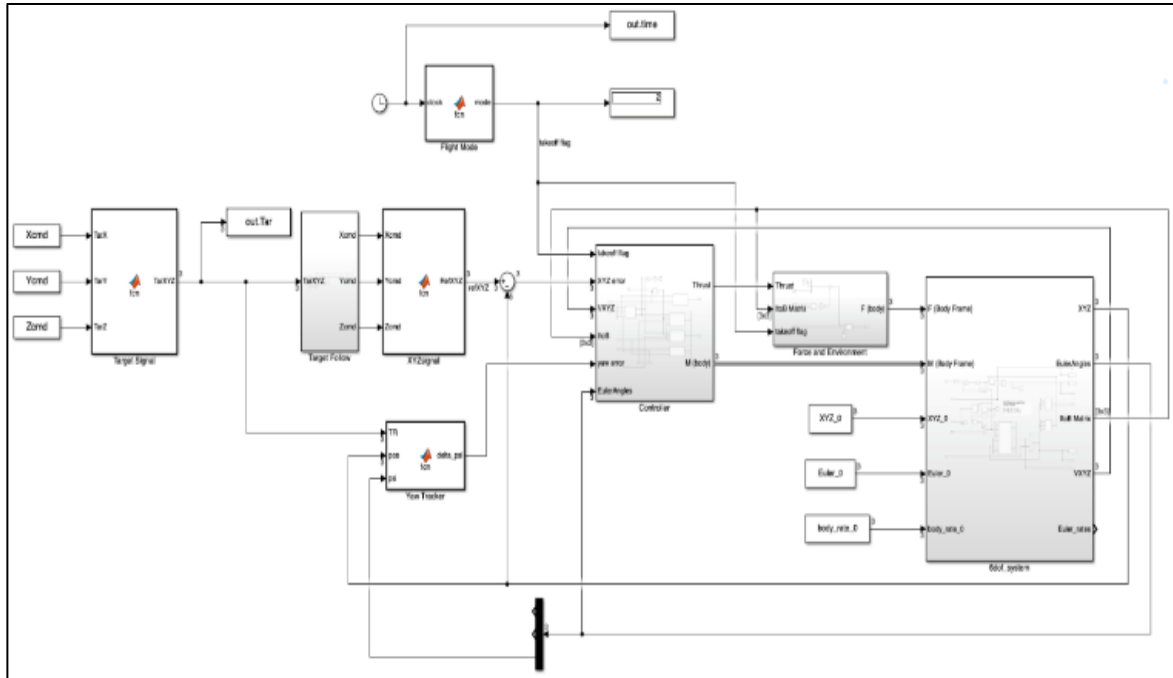
Figure 4.12 : Simulink model.

different values, z_sum will take the altitude specified in the second waypoint which is 3, and keep the rest of the arrays as zero during this interval.

In case of k > 2, we will generate a loop that updates the values of the three arrays based on the derivatives of x, y, and z and the time step 0.1 in order to calculate the position during these intervals.

➢ We generate the x, y, and z commands using the function (timeseries ( )) that takes the signal data from the previous arrays and associates them with the corresponding time values in t as the code shows.

➢ Implement control system:

The previous commands will be implemented in the Simulink model.

➢ 3D animation of the drone simulation:

➢ To visualize the drone, it is crucial to set up the figure and the axis limitations where the drone will appear.

```
2        figure;
3        xlimit = [-3 9];
4        ylimit = [-3 10];
5        zlimit = [0 9];
6        width = 750;
7        height = 650;
8        NewFigure(xlimit,ylimit,zlimit,-43,25,width,height);
```

Figure 4.13 : Figure's characteristics.

The NewFigure function serves to set up the figure properties, including the x, y, and z axes limits, view angle, and the width and height are the size of the figure window.

➢ We define a function that calculate the transfer function from the body frame to the inertial frame using the Euler angles as inputs.

```
1 ⊟    function m = matrixB2I(phi,theta,psi)
2           m = [cos(theta)*cos(psi), sin(phi)*sin(theta)*cos(psi)-cos(phi)*sin(psi),
3
4                                     cos(phi)*sin(theta)*cos(psi)+sin(phi)*sin(psi);
5               cos(theta)*sin(psi), sin(phi)*sin(theta)*sin(psi)+cos(phi)*cos(psi),
6
7                                     cos(phi)*sin(theta)*sin(psi)-sin(phi)*cos(psi);
8                 -sin(theta),                                  sin(phi)*cos(theta),
9
10                                                              cos(phi)*cos(theta)];
11      end
```

Figure 4.14 : Transfer function from the body frame to inertial frame.

➢ We use animated line to create a line with a width of 1 and a line style ':' , this line animates the waypoints positions (x, y, z).

➢ We define a function to animates the Euler angles, position and velocity of the drone. In addition,we will specify the body frame in our simulation by drawing three lines.

```
230  ⊟   function line = drawline(p1,p2,color,width)
231          pt1 ≡ p1
232          pt2 = pt1 + transpose(p2);
233          pts = [pt1;pt2];
234          line = plot3(pts(:,1), pts(:,2), pts(:,3),color,'LineWidth',width);
235      end
```

Figure 4.15 : lines function.

➢ After defining the function, we create the desired lines:

Line 1: represents the x body frame, colored in blue.

Line 2: represents the y body frame, colored in green.

Line 3: represents the z body frame, colored in red.

0.5: the drone's arm length.

```
104    line1 = drawline(XYZ,O_I(:,1),'b--',1.5)
105    line2 = drawline(XYZ,O_I(:,2),'g--',1.5)
106    line3 = drawline(XYZ,O_I(:,3),'r--',1.5)
```

Figure 4.16 : the desired lines.

We extend those lines to visualize the frame orientation.

```
109    frame1 = drawline(XYZ,0.5*O_I(:,1)+0.5*O_I(:,2),'black',2.5)
110    frame2 = drawline(XYZ,0.5*O_I(:,1)-0.5*O_I(:,2),'black',2.5)
111    frame3 = drawline(XYZ,-0.5*O_I(:,1)+0.5*O_I(:,2),'black',2.5)
112    frame4 = drawline(XYZ,-0.5*O_I(:,1)-0.5*O_I(:,2),'black',2.5)
```

Figure 4.17 : frame visualization.

We update the plot them and delete the lines representing the body frame at each time step.

```
160    for i = 1:length(t_plot)
161        if abs( t_plot(i) - t_section) < 0.0001
162            % Do Animation
163            subplot(1,2,1)
164            NewFigure([-3 3],[-1 5],[0 6],0,0,1200,600);
165            scatter3(TR(1),TR(2),TR(3),'filled','MarkerFaceColor','black'
166            Euler = EulerAngles(i,:)
167            XYZ = XYZs(i,:)
168            O = eye(3);
169            T_BtoI = matrixB2I(Euler(1),Euler(2),Euler(3));
170            O_I = T_BtoI*O
171            line1 = drawline(XYZ,O_I(:,1),'b')
172            line2 = drawline(XYZ,O_I(:,2),'g')
173            line3 = drawline(XYZ,O_I(:,3),'r')
```

Figure 4.18 : Drone's animation loop.

➢ We define a loop through each time step and checks if the current time step is close to the previous time section, if it is the animation is performed using the transformation matrix from the body to the initial frame we mentioned before.

Here is a diagram that resumes the simulation steps and process:
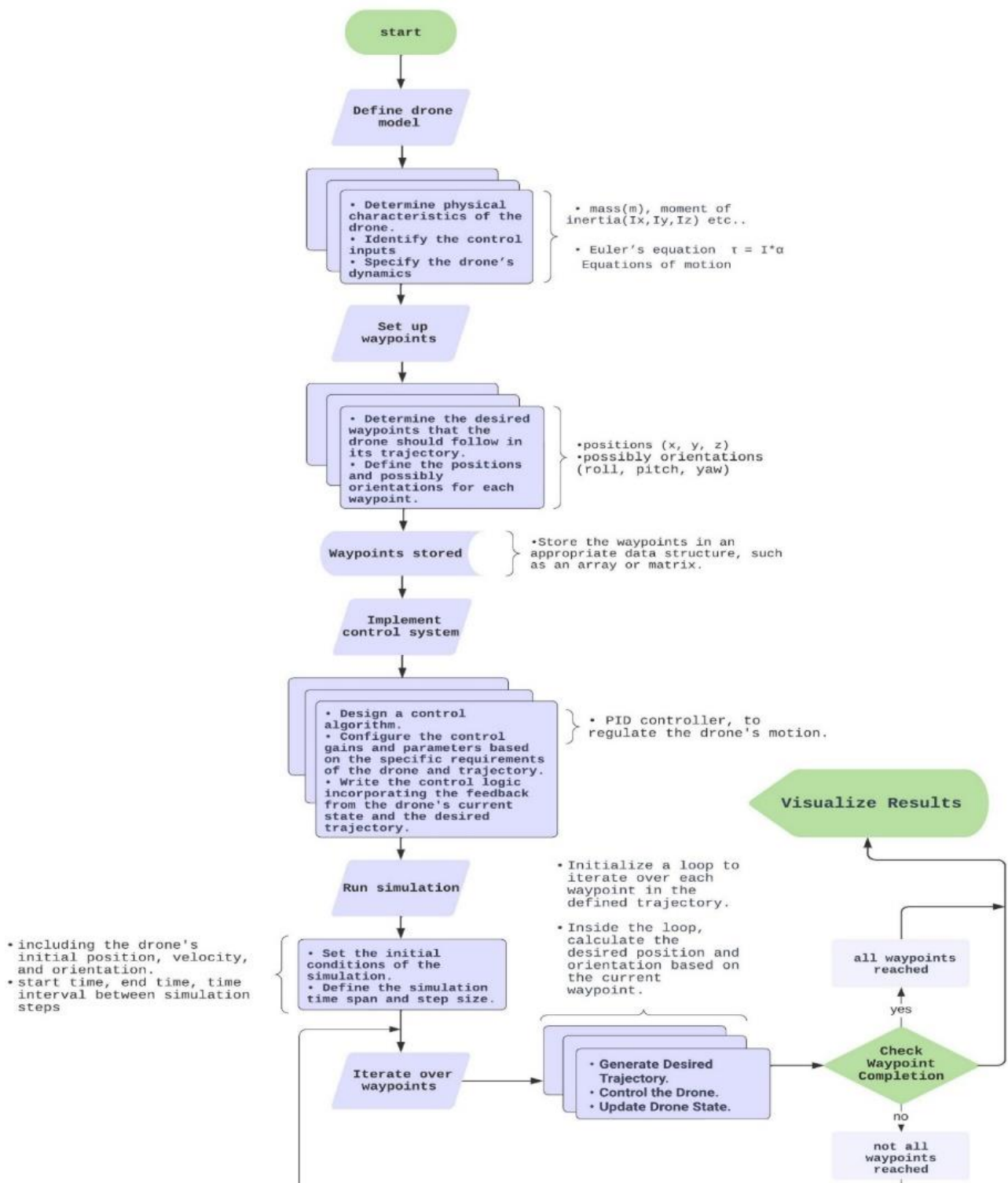
Figure4.19: Logigram of the drone's simulation.

3.6   Results and discussion of the drone's simulation:

The figures below represents the 3D drone's simulation:
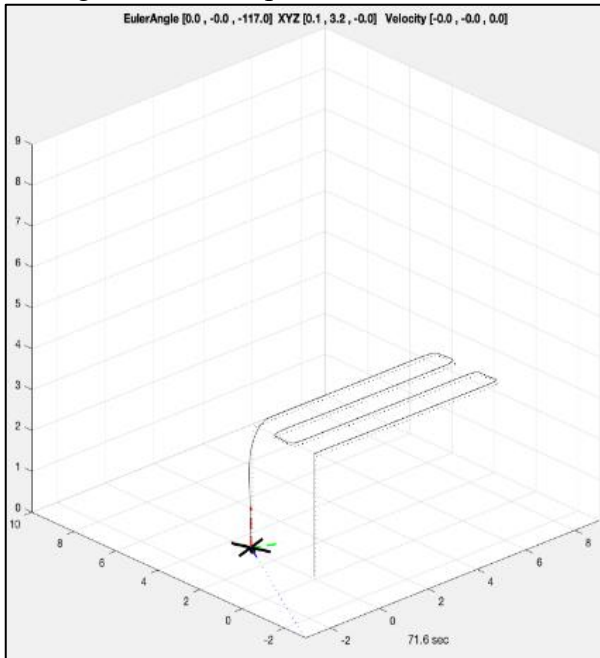
Figure4.20: Arrival point of the drone.   **Figure4.21:** The drone During the fly.
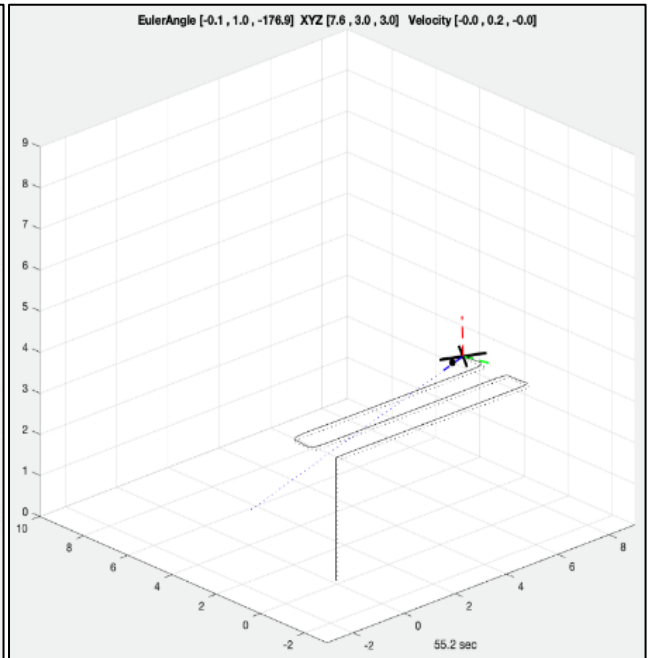
The following graphs represent the drone's behavior during the simulation:

➢   The figure below shows the variation of the drone's position with time:
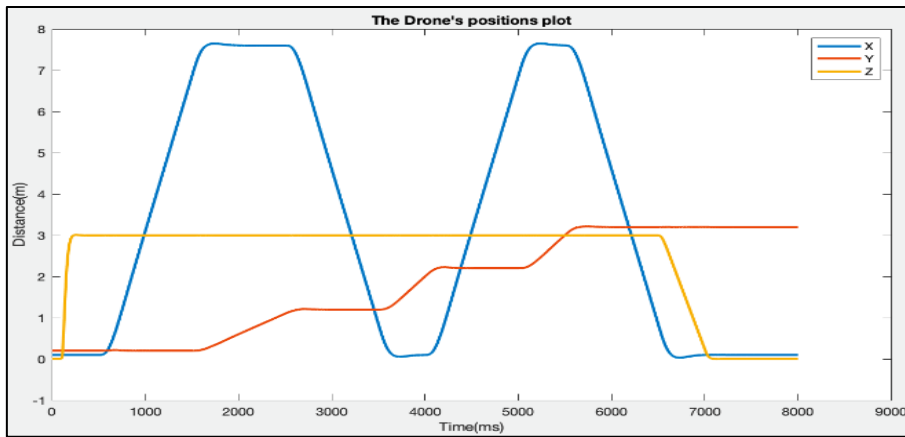
Figure4.22: Graph that represents the position's variation.

➢ The figure below shows the variation of the drone's velocity with time:

Figure 4.23: Graph representing the variation of velocity with time.
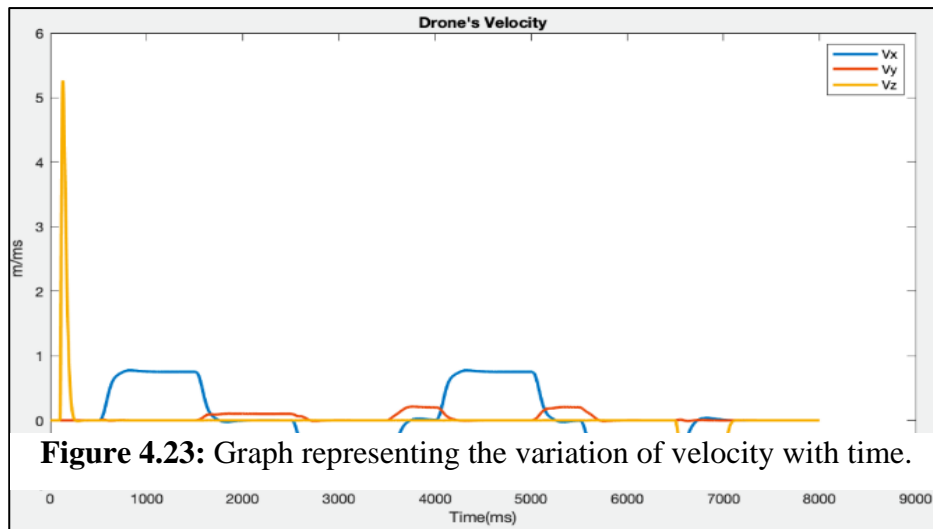
➢ The figure below shows the variation of the drone's attitude with time:
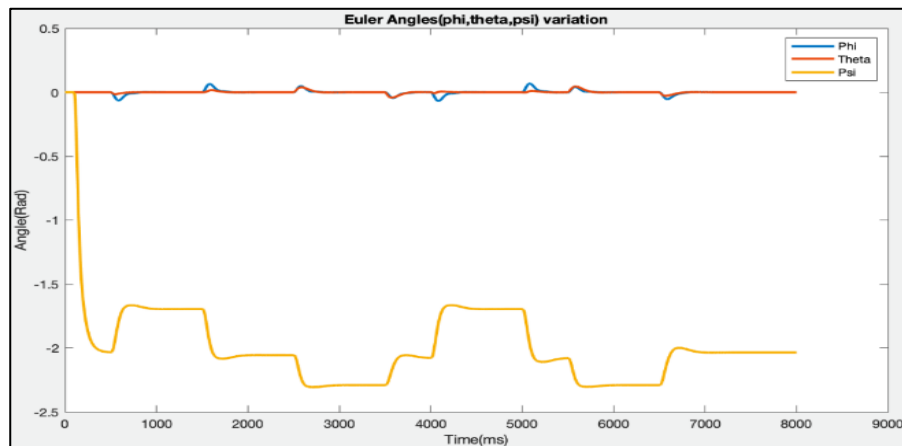
Figure 4.24: Graph representing the Euler angles variation.

Results obtained:

The simulation was executed to evaluate the trajectory of the drone that has predefined waypoints based on real measurements and through analysis of the photovoltaic power plant, specifying an example of one array. The simulation generated the desired trajectory accurately, providing the variation of the drone's positions, velocity, and Euler angles. As the two figures show, the drone successfully followed all the set waypoints and completed the predetermined trajectory.

3.6.1 Discussion of the results:

The simulation successfully modeled the drone and provided the drone's flight dynamic which consists of the variation of position, velocity, and Euler angles. As the graphs shows:

➢ the variation of the drone's position (x, y, z) is accurate with the predefined waypoints, each of the coordinate's variate as the predefined trajectory.

➢ The velocity at first was just on the z axis because it was the take-off phase, then we notice that the variation of this velocity stabilizes at the zero point during the rest of the trajectory until we enter the landing phase when the velocity on this axis variate in a negative way which means that the drone decreases the speed and go downward the z axis orientation. When we move in the same direction as the x-axis orientation the velocity in this last increase, then variate in the negative sense when the drone's moves in the opposite way and the same goes for the y-axis.

➢ Euler angles variation graph shows that the phi and theta angles have almost a similar small variation meanwhile the psi angle decrease and is not stable with time due to the gain tunes.

4.   IMAGE PROCESSING:

Following the collection of images captured by the drone during its inspection of photovoltaic arrays, it is imperative to detect any anomalies present within them. However, the manual process of analyzing the data collected by the drone can be time-consuming and error prone task.

In order to accomplish this task with a reduced time and more precision, we made a program using MATLAB that is based on comparing infrared images of the photovoltaic modules captured by the drone with a dataset of infrared images of solar modules downloaded on website named Kaggle. The dataset contains 20 000 images of photovoltaic cells with known defects such as hot spots, cracking, and delamination.
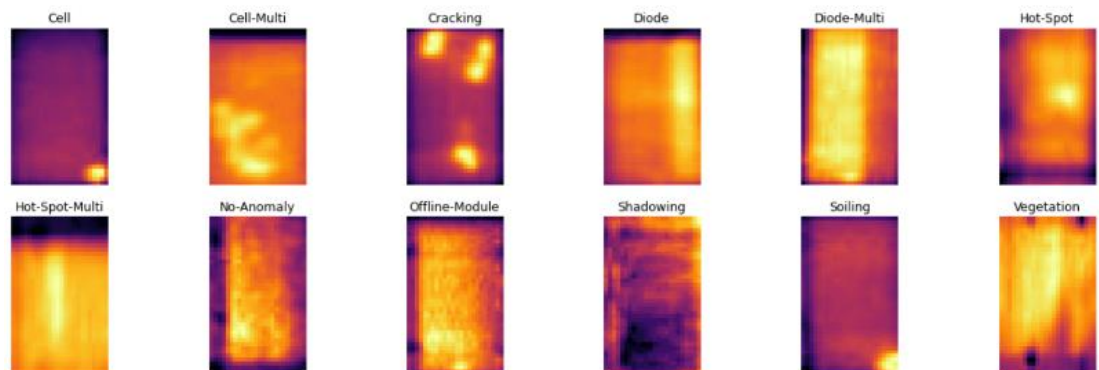
Figure4.25: Different anomalies present in the dataset**.**

The dataset, consisting of 20,000 cell images, has been classified into two categories: those with and without anomalies. The figures illustrating the anomalous cells present in the dataset are represented in Figure 11, and detailed in figure 12 bellow:

4.1   Method used and implementation of the program:

Our program is based on comparing images, for that we used the Structural Similarity Index (SSIM) function in our program because it provides a measure of structural similarity between two images. This method consists of comparing local patterns of pixel intensities and takes into consideration luminance, contrast, and structure information. This is important because the images are infrared and the anomaly in the photovoltaic cells can be represented as a discoloration as in hot spots or a change in texture as in cracking, which can be captured by the SSIM metric.

The Structural Similarity Index (SSIM) metric extracts 3 key *features* from an image, which
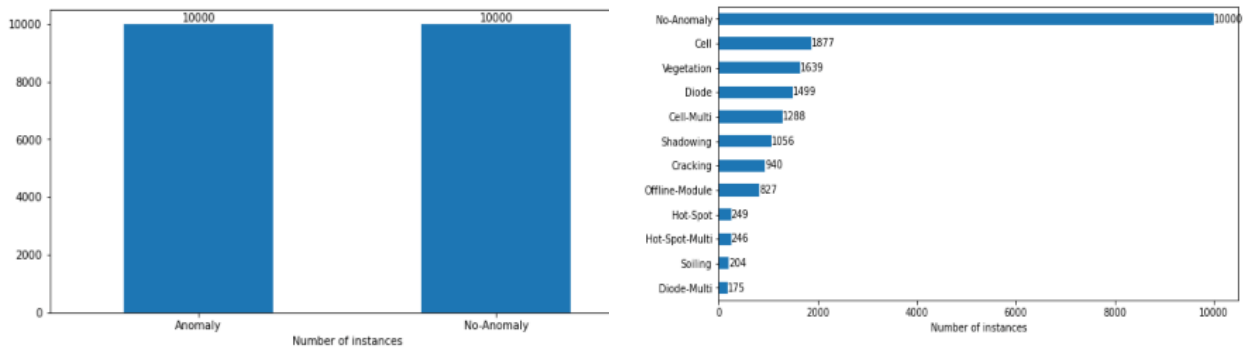
Figure 4.26: Graphs illustrating different anomalies present in the dataset

the comparison between two images will be based on them [84]:

 ➢ Luminance.
 ➢ Contrast.
 ➢ Structure.

Here is a figure that shows how the SSIM works based on the x,y as in inputs of the image and the three key features we already mentioned.

The equation of the similarity function is given by

$$SSIM = \frac{(2\mu_x\mu_y+C_1)(2\sigma_{xy}+C_2)}{(\mu_x{}^2+\mu_y{}^2+C_1)(\sigma_x{}^2+\sigma_y{}^2+C_2)}$$
(4.24)
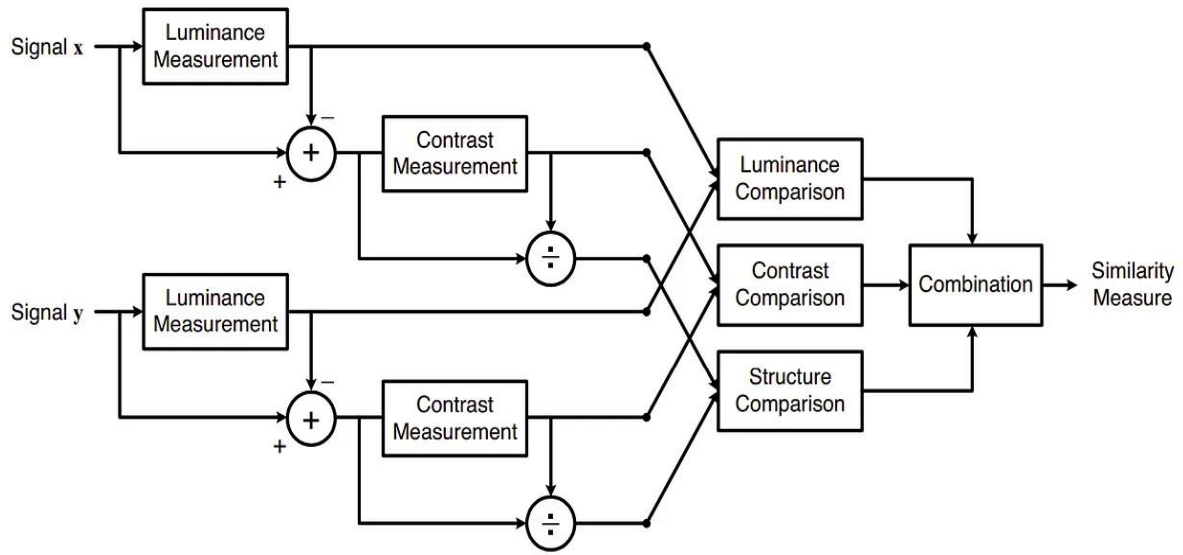
Figure 4.27: Diagram of the structural similarity (SSIM) measurement system [84].

To enable working with the dataset, we added 152 images that encompass various anomalies to an Excel spreadsheet in a table format named (Defects) consisting of two columns. The first column was dedicated to image numbering while the second listed the specific anomalies present within each image. We have stored the 152 images in a folder named Dataset, and the Images captured in another folder named ImgTaken.

N-images	Defect type
13357	No-anomaly
13607	No-anomaly
10887	No-anomaly
10881	No-anomaly
13603	No-anomaly
10886	No-anomaly
10888	No-anomaly
12832	No-anomaly
18515	No-anomaly
16890	No-anomaly
19330	No-anomaly
6797	Hot-spot
6950	Hot-spot
6951	Hot-spot
6953	Hot-spot
6952	Hot-spot
6860	Hot-spot
6867	Hot-spot
6861	Hot-spot

Dataset

ImgTaken

Figure 4.28: Excel dataset table.

4.2   Program implementation:

After we prepared the folders and the dataset needed for this work, we developed the next program:

➤   We firstly should define the paths to the two image folders containing the captured images and the Dataset images. These are stored as strings in variables.

➤   We next imported the EXCEL table to MATLAB by the function "load" that we will use after as a reference table to know the anomaly related to the image treated.

➤   After specifying the image paths, we should read the image stored inside, for that we used "imread" function from MATLAB's image processing toolbox.

➤   Since we are comparing one image with the whole "Dataset" we will need to read all images stored in this last. For that, we used "dir()" command along with "fullfile()" method to get information about all available images that are '.jpg' files within Dataset folder that we indicated its path at first.

➤   We then extract the number of images present on the folder by using the function "numel()" to generate a loop which will begin by i = 1 to the number of images in the Dataset folder which is 152 image.

➤   Before generating the loop, we initialized two empty arrays which we will use to store the similarity values in it.

➤   We then generate a loop that will iterate over every image present in Dataset folder to read each one individually before calculating its similarity with our captured image taken earlier via the function "imread()".

For each comparison made between the captured/Dataset image, we calculate their Structural Similarity Index (SSIM) value using the MATLAB built-in function called "ssim" which returns a scalar score quantifying how similar the two images are based on their structural information.

➤   We after that store the SSIM results in the arrays we initialized previously.

➤   Next, we extract the Index position of the image with the highest similarity score using the "max()" function and show the results.

➤   In a final program block, we use the downloaded EXCEL table named Defects to find the row corresponding to the matching image and display the result adding a figure to show the captured image and the most similar image to this last.

Here is an extract of the MATLAB program:

```
1    % Define paths to folders containing reference and test images
2    ref_folder_path = '/Users/mac/Desktop/program/data/ImgTaken/';
3    test_folder_path = '/Users/mac/Desktop/program/data/Dataset/';
4
5    % Read Taken image from its path
6    imageTaken = 'im19.jpg';
7    ref_img_path = fullfile(ref_folder_path, imageTaken);
8    ref_img = imread(ref_img_path);
9
10   % Get all files from second path
11   test_imgs_dir = dir(fullfile(test_folder_path, '*.jpg'));
12
13   % Initialize variables for storing similarity values
14   sim_values_allimgs  = zeros(length(test_imgs_dir), 1);
15   file_names_allimgs  = cell(length(test_imgs_dir), 1);
16
17 ⊞ for i=1:length(test_imgs_dir) […]
29
30   % Find index of maximum value of similarities array.
31   [max_sim_value, max_sim_index]  = max(sim_values_allimgs);
```

```
45   % Find the row with the matching Nimages value
46   row = Defects(Defects.Nimages == I, :);
47
48   % Display the entire row
49   disp(row);
50
51   imagePath = sprintf('/Users/mac/Desktop/program/data/Dataset/%d.jpg'
52
53   % Load and display the corresponding image
54   image = imread(imagePath);
55   imshow(image);
56   subplot(1, 2, 2);
57   imshow(image);
58   title('Most Similar Image');
59
60
61   subplot(1, 2, 1);
62   imshow(i2);
63   title('Image Taken');
```

Figure 4.29 : an extract of the image processing program (1).   **Figure 4.30 :** an extract of the image processing program (2).

To have a clearer idea of our program process we have made an organigram that simplifies the steps:
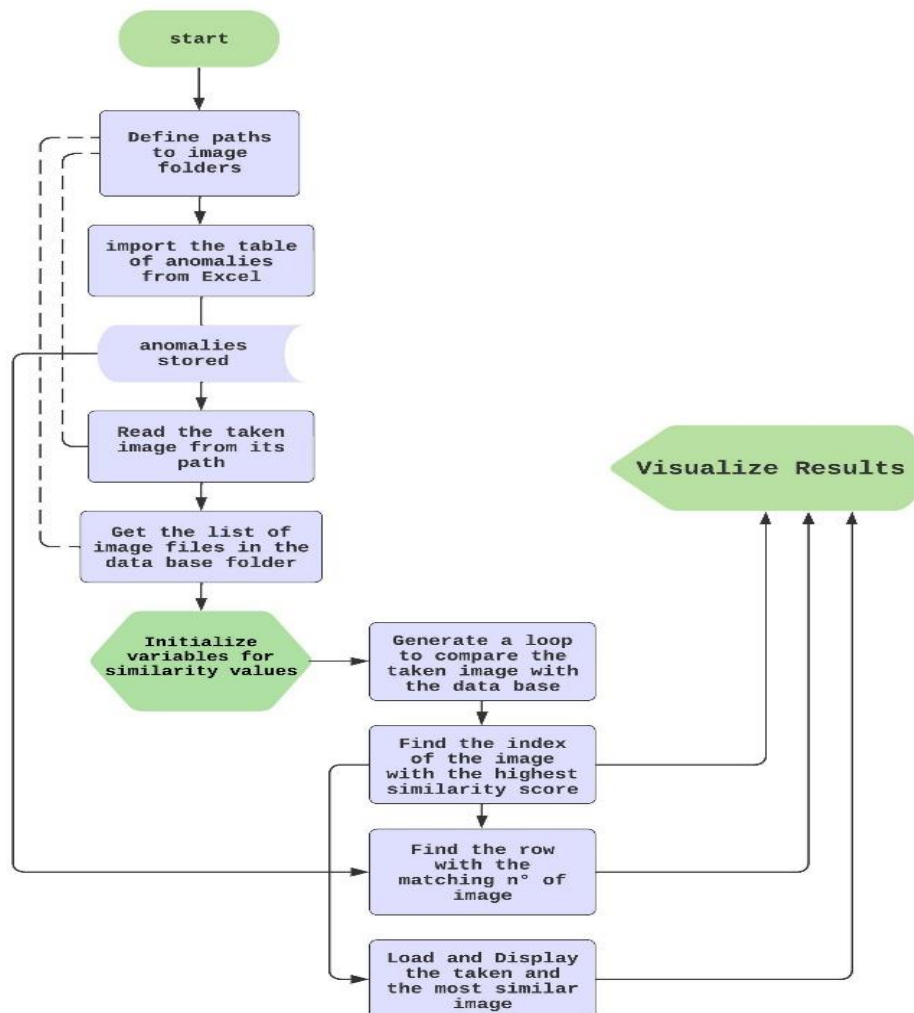
Figure 4.31 : Image processing using SSIM organigram.

4.3   Results obtained:

To validate the program, we chose images from the main dataset that contains 20 000 images. And we compared them with the 152 different images that we extracted from the main dataset.

Here are the results we obtained from testing the program with 3 images and their validation:
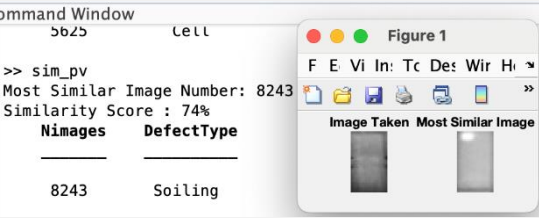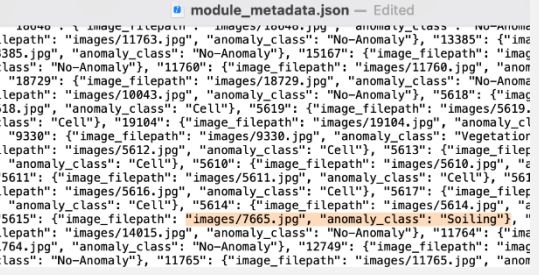
Image number	The result obtained	The validation of the results
7118		
11542		
7665		

Table 4.1 : Image processing results table.

As we can see from the table, pointing in the anomalies and their type, image number 7118 and 7665 has an anomaly, while the image 11542 has no anomalies. When we compare those results with their dataset information, we see that the three of them had the same results as their information.

When we look at the similarity score, the three images have a high similarity score greater than 60%, which is a good result.

4.4   Discussion of the results:

➢ Based on the results, our program successfully calculates the Structural Similarity Metric values between the taken images and all the dataset images. It identifies the image with the highest similarity value as the most similar image and the highest similarity score represents how closely the dataset image resembles the taken image. This image is then displayed alongside the taken image for visual comparison, and since the primary goal of detecting photovoltaic faults is to identify any anomalies or irregularities in the panel's images that m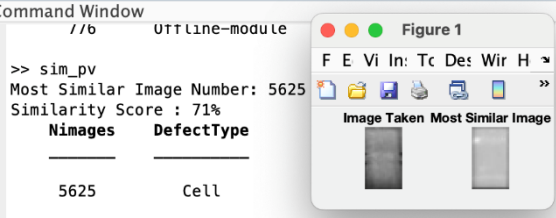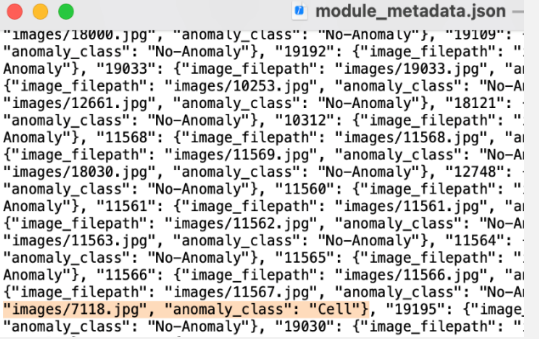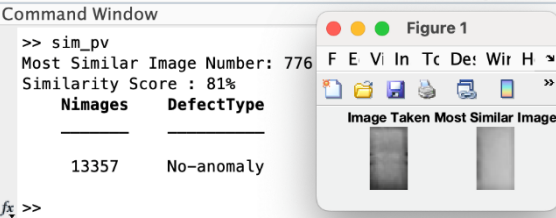ay indicate potential issues in them, by using the Defects table that contains the different possible anomalies in the photovoltaic field and their images, inserting the number of the most similar image to the taken image, we obtain the possible anomaly related to the taken image.

➢ The similarity score represents the percentage of similarity between the two images. It ranges from 0 to 100 %, with 100 % indicating a perfect similarity. The higher the similarity score, the more structurally similar the images are.

➢ Our program according to this and the results has successfully extracted the exact anomalies with a high score of similarity. However, a largest dataset would improve the program's performance to have a more precise test of the method we utilized in this program. The Dataset should cover more anomalies taking in consideration the weather conditions, lighting, and other faults to ensure the algorithm's robustness.

5.   CONCLUSION:

In conclusion, the successful reproduction of the predefined trajectory, along with the precise drone parameters variation, highlights the reliability and effectiveness of this simulation which makes MATLAB a great platform for aircraft dynamics and trajectory generation applications.

In another part, we presented our image processing program that uses drones to detect anomalies on photovoltaic panels through a comparison with a dataset using the Structural Similarity Metric. Our experimental results indicate the potential of using the SSIM algorithm for detecting photovoltaic faults, and that our program was able to accurately identify anomalies present in the captured images with a high similarity score.

However, further optimizations, and particularly in gain tuning are required to improve the attitude stabilization in future simulations. In addition, researches are needed to optimize the approach, define a largest dataset of fault types, the use of CNN to be more efficient, and establish an appropriate threshold. By addressing these aspects, we can enhance the detection accuracy and contribute to the development of more reliable and efficient fault detection techniques in photovoltaic systems.

General conclusion

General conclusion:

We conclude that the obtained results are focused on the inspection and detection of faults in photovoltaic systems using drones. This work is an outcome of a whole comprehensive university curriculum that equipped us with essential knowledge in navigation, flight mechanism, and avionics systems.

This master's thesis aims to study and develop an algorithm of detection an efficient and cost-effective method for inspecting and detecting faults in photovoltaic systems using drone technology. The primary goal was to utilize the advantages offered by drones, such as their ability to cover large areas quickly, capture high-quality images, and reduce inspection costs while addressing some limitations associated with traditional methods. By combining drone technology with image processing techniques, the study aimed to provide a solution that can efficiently detect potential malfunctions or anomalies in photovoltaic arrays.

We made a theoretical background on renewable energy, with a specific focus on Algeria's solar energy projects. We also explored the history and principles of photovoltaic cells and drones to gain a better understanding of their applications in inspecting photovoltaic systems.

We then discussed traditional and new methods used for photovoltaic system inspection, highlighting some limitations associated with current approaches. Additionally, we conducted simulations to study the behavior of two different photovoltaic stations under various conditions such as irradiation and shading.

As a solution to these challenges, we used drone technology to efficiently screen large-scale photovoltaic arrays. Next, we simulated the drone trajectory in MATLAB software successfully while capturing high-quality images during its flight over the arrays. Our study relied on image processing techniques such as comparison with datasets to accurately detect any potential failures or anomalies.

Globally, this research demonstrated how innovative drone technology can be utilized effectively for improving inspections in large-scale renewable energy facilities like Photovoltaic systems thus contributing towards sustainable development efforts globally by promoting effective monitoring mechanisms leading towards cost savings while reducing carbon emissions affecting our environment positively.

All these features made the system robust and feasible to provide the required contribution to the field of avionics, specifically in the domain of photovoltaic system inspections. By integrating drone technology and leveraging its capabilities, we have demonstrated the potential for enhanced fault detection and

inspection efficiency. The research conducted in each chapter has expanded our understanding of photovoltaics, established effective fault detection methods, simulated and optimized the inspection process, and proposed an innovative solution that paves the way for improved reliability and safety in photovoltaic system inspections.

Finally, further research can focus on the integration of artificial intelligence and machine learning algorithms to enhance fault detection capabilities and automate the inspection process. Additionally, exploring the feasibility of deploying drones in large-scale photovoltaic installations and optimizing their flight paths for efficient inspections would be valuable avenues for future investigations.

With the potential to revolutionize the industry by improving inspection efficiency, ensuring optimal performance, and preventing hazards, the application of drones in this domain holds great promise for a sustainable and energy-efficient future

REFERENCES

[1]   The Harvard Law School Forum on Corporate Governance. (2021, March 2). *Climate Risk and the Transition to a Low-Carbon Economy.* https://corpgov.law.harvard.edu/2021/03/02/climate-risk-and-the-transition-to-a-low-carbon-economy/

[2]   Pistorius, M., & Pistorius, M. (2021). New tool to monitor energy transition progress of French regions. *www.euractiv.com.* https://www.euractiv.com/section/economy-jobs/news/new-tool-to-monitor-energy-transition-progress-of-french-regions/

[3]   International Trade Administration U.S. Department of Commerce. (2023, January 31). *Algeria - Renewable Energy.* International Trade Administration | Trade.gov. https://www.trade.gov/country-commercial-guides/algeria-renewable-energy#:~:text=Regarding%20solar%20power%20potential%2C%20Algeria,year%20in%20its%20desert%20regions

[4]   Tiwari, A., & Jain, S. (2016). A review on Solar Drying of Agricultural Produce. *ResearchGate.* https://www.researchgate.net/publication/333080865_A_review_on_Solar_Drying_of_Agricultural_Produce

[5]   Kermadi, M., & Berkouk, E. M. (2015). Techno-economic feasibility study for the use of photovoltaic energy on the south-east algerian farms. *ResearchGate.* https://www.researchgate.net/publication/309721990_Techno-economic_feasibility_study_for_the_use_of_photovoltaic_energy_on_the_south-east_algerian_farms

[6]   International Trade Administration U.S. Department of Commerce. (2023, January 31). *Algeria - Renewable Energy*. International Trade Administration | Trade.gov. https://www.trade.gov/country-commercial-guides/algeria-renewable energy#:~:text=Regarding%20solar%20power%20potential%2C%20Algeria,year%20in%20its%20desert%20regions

[7]   *Algeria charts a path for renewable energy sector development*. (n.d.). Middle East Institute. https://www.mei.edu/publications/algeria-charts-path-renewable-energy-sector-development

[8]   SKTM & Sonelgaz (Directors). (2018). projets réalisés dans le cadre du programme national des énergies renouvelables. In *https://interieur.gov.dz/index.php/fr/*. ministère de l'Intérieur des Collectivités Locales et de l'Aménagement du Territoire.

[9]   *Solar Energy*. (n.d.). Otec. https://fr.otec-engineering.com/expertises/Solar-Energy

[10]   Mertens, K. (2018). *Photovoltaics: Fundamentals, Technology, and Practice*. John Wiley & Sons.

[11]   École de technologie supérieure. (n.d.). *Amélioration de l'algorithme MPPT pour un système PV par l'intégration des nouvelles techniques basées sur l'intelligence artificielle - Espace ETS*. https://espace.etsmtl.ca/id/eprint/3049

[12]   *Solar Power System Kits • Solar Panel Kits*. (n.d.). https://www.mrsolar.com/solar-power-system-kits/

[13]   B., a. T. Y., M., [MAAYOUF Ikram]. (12017 B.C.E.). *photovoltaiques B., A. T. Y. Mohamed "Centre Universitaire," Belhadj Bouchaib, Ain-Temouchent (2017)*. "Centre Universitaire," Belhadj Bouchaib, Ain-Temouchent.

[14]   HENNOUS, C., & AIT-ALLALA, K. (2008). *DIMENSIONNEMENT ET INSTALLATION D'UN SYSTEME PHOTOVOLTAIQUE (APPLICATION A LA F.G.E.I.)*. FACULTE DE GENIE ELECTRIQUE ET DE L'INFORMATIQUE DEPARTEMENT D'ELECTRONIQUE.

[15]   Asrmeta, A. (2021). Solar cells, their construction, and working. *ASRMETA*. https://www.asrmeta.com/solar-cells-their-construction-and-working/

[16]   Smets, A., Jäger, K., Isabella, O., Van Swaaij, R., & Zeman, M. (2016). *Solar Energy: The Physics and Engineering of Photovoltaic Conversion, Technologies and Systems*. Uit Cambridge Limited.

[17]   Wang, T., & Tsai, S. Y. (2018). Solar Panel Supplier Selection for the Photovoltaic System Design by Using Fuzzy Multi-Criteria Decision Making (MCDM) Approaches. *Energies*, *11*(8), 1989. https://doi.org/10.3390/en11081989

[18]   Kurukuru, V. S. B., Blaabjerg, F., Khan, M. Z. A., & Haque, A. (2020). A Novel Fault Classification Approach for Photovoltaic Systems. *Energies*, *13*(2), 308. https://doi.org/10.3390/en13020308

[19]   Haque, A., Kurukuru, V. S. B., Khan, M. Z. A., Khan, I., & Jaffery, Z. A. (2019). Fault diagnosis of Photovoltaic Modules. *Energy Science & Engineering*, *7*(3), 622–644. https://doi.org/10.1002/ese3.255

[20]   Singh, N. K., Muthukrishnan, P., & Sanpini, S. (2019). *Industrial System Engineering for Drones: A Guide with Best Practices for Designing*. Apress.

[21]   Skoog, A. I. (2010). The Alfred Nobel rocket camera. An early aerial photography attempt. *Acta Astronautica*, *66*(3–4), 624–635. https://doi.org/10.1016/j.actaastro.2009.06.011

[22]   Kozera, C. A. (2018). Military Use of Unmanned Aerial Vehicles – A Historical Study. *Safety & Defense*, *4*, 17–21. https://doi.org/10.37105/sd.4

[23] Skoog, A. I. (2010). The Alfred Nobel rocket camera. An early aerial photography attempt. *Acta Astronautica*, *66*(3–4), 624–635. https://doi.org/10.1016/j.actaastro.2009.06.011

[24] *All the World's Helicopters and Rotorcraft - the most complete helicopter collection in the world. Helicopters, autogyros, tilt-rotors, tilt-wings etc.* (n.d.). http://www.aviastar.org/

[25] *America's First Military Helicopter: The Flying Octopus*. (n.d.). National Air and Space Museum. https://airandspace.si.edu/events/americas-first-military-helicopter-flying-octopus

[26] De Thèse Boudjema, F. D. (2022). *Système de vision pour la commande d'un UAV « Unmanned aerial vehicle », type quadrotor*. http://repository.enp.edu.dz/jspui/handle/123456789/10698

[27] *Parrot Bebop 2 Drone*. (n.d.). Microsoft Store. https://www.microsoft.com/en-ca/d/parrot-bebop-2-drone/8v4c86w1b51d

[28] Kardasz, P., Doskocz, J., Hejduk, M., Wiejkut, P., & Zarzycki, H. (2016). Drones and Possibilities of Their Using. *Journal of Civil & Environmental Engineering*, *6*(3). https://doi.org/10.4172/2165-784x.1000233

[29] Kardasz, P., Doskocz, J., Hejduk, M., Wiejkut, P., & Zarzycki, H. (2016). Drones and Possibilities of Their Using. *Journal of Civil & Environmental Engineering*, *6*(3). https://doi.org/10.4172/2165-784x.1000233

[30] Van Oort, J. (2018). *COORDINATE SYSTEM INVARIANT QUADROTOR CONTROL*.

[31] Helal, A., Rouini, H., & Djomai, R. (2014). *Système rembarqué et mobile*.

https://fr.scribd.com/document/511020102/pfe-drone-voir-conception-1

[32] Gibiansky, A. (n.d.). *Quadcopter Dynamics and Simulation - Andrew Gibiansky*. https://andrew.gibiansky.com/blog/physics/quadcopter-dynamics/

[33] Gibiansky, A. (n.d.-b). *Quadcopter Dynamics and Simulation - Andrew Gibiansky*. https://andrew.gibiansky.com/blog/physics/quadcopter-dynamics/

[34] Hussein, A., & Abdalla, R. (2017). Autopilot Design for a Quadcopter. *ResearchGate*. https://doi.org/10.13140/RG.2.2.17020.80008

[35] Abbas, N. H., & Sami, A. (2018). Tuning of PID Controllers for Quadcopter System using Cultural Exchange Imperialist Competitive Algorithm. *Maǧallaẗ Al-handasaẗ*, *24*(2), 80–99. https://doi.org/10.31026/j.eng.2018.02.06

[36] *Flying drone with the motors spinning out and not in*. (2022, May 25). ArduPilot Discourse. https://discuss.ardupilot.org/t/flying-drone-with-the-motors-spinning-out-and-not-in/85998

[37] Kardasz, P., Doskocz, J., Hejduk, M., Wiejkut, P., & Zarzycki, H. (2016c). Drones and Possibilities of Their Using. *Journal of Civil & Environmental Engineering*, *6*(3). https://doi.org/10.4172/2165-784x.1000233

[38] Chmaj, G., & Selvaraj, H. (2015). Distributed Processing Applications for UAV/drones: A Survey. In *Advances in intelligent systems and computing* (pp. 449–454). Springer Nature. https://doi.org/10.1007/978-3-319-08422-0_66

[39] *Renewable Energy Policy | Wind & Solar Regulatory Compliance*. (n.d.). https://www.esri.com/en-us/industries/renewables/segments/policy-compliance

[40] *SEM-SOLAR*. (n.d.). http://www.sem-solar.co.jp/en/services/optional

[41]   Solar Electric Power Generation. (2006). In *Springer eBooks*. https://doi.org/10.1007/978-3-540-31346-5

[42]   *Manufacturer of test and measurement equipment | HT Instruments*. (n.d.). https://www.ht-instruments.com/en/

[43]   *PVCHECKs | Commissioning and Maintenance | HT Instruments*. (n.d.). https://www.ht-instruments.com/en/products/photovoltaic-testers/commissioning-and-maintenance/pvchecks/

[44]   *Manufacturer of Test and Measurement equipment | HT Instruments*. (n.d.). https://www.ht-instruments.com/

[45]   Beale, A., & Kuchta, D. (2022, November 18). *Standard Test Conditions (STC) for Solar Panels*. https://footprinthero.com/standard-test-conditions

[46]   Reon. (2023). Performance Evaluation of Solar Plants using I-V Curve Tracer. *Energy Company in Pakistan*. https://reonenergy.com/performance-evaluation-of-solar-plants-using-i-v-curve-tracer/

[47]   *IV Curve | PVEducation*. (n.d.). https://www.pveducation.org/pvcdrom/solar-cell-operation/iv-curve

[48]   *What is I-V Curve Tracing?* (n.d.). Fluke Resource Center. https://www.fluke.com/en-us/learn/blog/renewable-energy/iv-curve-tracing

[49]   *Fluke SMFT-1000 Solar PV Multifunction Tester and I-V Curve Tracer*. (n.d.). Test Meter Group Ltd. https://www.test-meter.co.uk/fluke-smft-1000-solar-pv-multifunction-tester-and-i-v-curve-tracer

[50]   *Building an effective meteorological station for solar PV*. (2022, September 29). Pv Magazine -

         Photovoltaics Markets and Technology. https://www.pv-magazine.com/2022/09/29/building-an-

         effective-meteorological-station-for-solar-pv/

[51]   Menichini, V. (2023). Weather stations for a solar plant in Brazil. *LSI LASTEM*. https://www.lsi-

         lastem.com/case-studies/weather-stations-for-a-solar-plant-of-223-mw-capacity-in-brazil/

[52]   *Solar (PV) Power Monitoring - Weather Monitoring Sensors Stations, Size: 4m - PDF Catalogue*.

         (n.d.).   https://pdf.indiamart.com/impdf/21709848573/MY-96728416/solar-pv-power-monitoring-

         weather-monitoring-sensors-stations.pdf

[53]   Fernández-Solas, Á., Micheli, L., Almonacid, F., & Fernández, E. (2022). Indoor validation of a

         multiwavelength measurement approach to estimate soiling losses in photovoltaic modules. *Solar

         Energy*, *241*, 584–591. https://doi.org/10.1016/j.solener.2022.06.036

[54]   Team, O. H. B. (2021). The DustIQ arrives at the Green Energy Park. *OTT Blog*.

         https://blog.otthydromet.com/en/the-dustiq-arrives-at-the-green-energy-park/

[55]   Seven Sensor - ArgeSim Group. (2021, September 16). *PV Module Temperature Sensor Selection

         According to IEC 61724-1*. Seven Sensor. https://www.sevensensor.com/pv-module-temperature-

         sensor-selection-according-to-iec-61724-1

[56]   Sensor, S. (2022). PV Module Temperature Sensor Selection According to IEC 61724-1. *Seven

         Sensor*.   https://www.sevensensor.com/pv-module-temperature-sensor-selection-according-to-iec-

         61724-1

[57]   Sensor, S. (2022b). PV Module Temperature Sensor Selection According to IEC 61724-1. *Seven Sensor*.   https://www.sevensensor.com/pv-module-temperature-sensor-selection-according-to-iec-61724-1

[58]   Concrete5. (2022). *Solar PV MET Stations* (Datasouth, Ed.). Power Wise Systems. https://www.powerwisesystems.com/products/pv-monitors/

[59]   *MET Stations for Large PV*. (n.d.). https://www.powerwisesystems.com/products/pv-monitors/

[60]   Dhoke, A., Sharma, R., & Saha, T. K. (2019). An approach for fault detection and location in solar PV systems. *Solar Energy*, *194*, 197–208. https://doi.org/10.1016/j.solener.2019.10.052

[61]   Juan, R. O. S., & Kim, J. (2020). *Photovoltaic Cell Defect Detection Model based-on Extracted Electroluminescence Images using SVM Classifier*. https://doi.org/10.1109/icaiic48513.2020.9065065

[62]   The Fundamentals and Applications of Light-Emitting Diodes. (2020). In *Elsevier eBooks*. https://doi.org/10.1016/c2019-0-00273-7

[63]   Henry, C. S. (2014). Electron-hole recombination [Dataset]. In *AccessScience*. https://doi.org/10.1036/1097-8542.224150

[64]   Mantel, C., Villebro, F., Benatto, G. a. D. R., Parikh, H. R., Wendlandt, S., Hossain, K. M., Poulsen, P. B., Spataru, S., Sera, D., & Forchhammer, S. (2019). *Machine learning prediction of defect types for electroluminescence images of photovoltaic panels*. https://doi.org/10.1117/12.2528440

[65]   Demirci, M., Beşli, N., & Gümüşçü, A. (2021). Efficient deep feature extraction and classification for identifying defective photovoltaic module cells in Electroluminescence images. *Expert Systems With Applications*, *175*, 114810. https://doi.org/10.1016/j.eswa.2021.114810

[66]   Demirci, M., Besli, N., & Gümüşçü, A. (2019b). Defective PV Cell Detection Using Deep Transfer Learning   and   EL   Imaging.   *ResearchGate*. https://www.researchgate.net/publication/344238806_Defective_PV_Cell_Detection_Using_Deep _Transfer_Learning_and_EL_Imaging

[67]   Demirci, M., Besli, N., & Gümüşçü, A. (2019). Defective PV Cell Detection Using Deep Transfer Learning   and   EL   Imaging.   *ResearchGate*. https://www.researchgate.net/publication/344238806_Defective_PV_Cell_Detection_Using_Deep _Transfer_Learning_and_EL_Imaging

[68]   Demirci, M., Besli, N., & Gümüşçü, A. (2019c). Defective PV Cell Detection Using Deep Transfer Learning   and   EL   Imaging.   *ResearchGate*. https://www.researchgate.net/publication/344238806_Defective_PV_Cell_Detection_Using_Deep _Transfer_Learning_and_EL_Imaging

[69]   Ramírez, I. S., Das, B., & Márquez, F. P. G. (2021). Fault detection and diagnosis in photovoltaic panels by radiometric sensors embedded in unmanned aerial vehicles. *Progress in Photovoltaics*, *30*(3), 240–256. https://doi.org/10.1002/pip.3479

[70]   De Oliveira, A. L., Aghaei, M., & Rüther, R. (2022). Automatic Inspection of Photovoltaic Power Plants   Using   Aerial   Infrared   Thermography: A   Review.   *Energies*,   *15*(6),   2055. https://doi.org/10.3390/en15062055

[71]   Fotovoltaica UFSC, & Aghaei, Dr. M. (2017). *"Novel Methods in Control & Monitoring of Photovoltaic Systems."*

[72]   Henry, C. S., Poudel, S., Lee, S., & Jeong, H. S. (2020). Automatic Detection System of Deteriorated PV Modules Using Drone with Thermal Camera. *Applied Sciences*, *10*(11), 3802. https://doi.org/10.3390/app10113802

[73]   Henry, C. S., Poudel, S., Lee, S., & Jeong, H. S. (2020b). Automatic Detection System of Deteriorated PV Modules Using Drone with Thermal Camera. *Applied Sciences*, *10*(11), 3802. https://doi.org/10.3390/app10113802

[74]   Ramírez, I. S., Das, B., & Márquez, F. P. G. (2021b). Fault detection and diagnosis in photovoltaic panels by radiometric sensors embedded in unmanned aerial vehicles. *Progress in Photovoltaics*, *30*(3), 240–256. https://doi.org/10.1002/pip.3479

[75]   Montanez, L. E., Valent´ın-Coronado, L. M., Moctezuma, D., & Flores, G. (2020). *Photovoltaic module segmentation and thermal analysis tool from thermal images*. IEEE.

[76]   Venkatesh, S. N., Jeyavadhanam, B. R., Sizkouhi, A. M. M., Esmailifar, S., Aghaei, M., & Sugumaran, V. (2022). Automatic detection of visual faults on photovoltaic modules using deep ensemble learning network. *Energy Reports*, *8*, 14382–14395. https://doi.org/10.1016/j.egyr.2022.10.427

[77]   De Oliveira, A. K. V., Aghaei, M., & Rüther, R. (2019). Automatic Fault Detection of Photovoltaic Arrays by Convolutional Neural Networks During Aerial Infrared. . . *ResearchGate*.

[78]   *Fig. 3. An overview of the zones segmentation's steps in PV module. . .* (n.d.). ResearchGate. https://www.researchgate.net/figure/An-overview-of-the-zones-segmentations-steps-in-PV-module-extraction-engine_fig3_351969085

[79] De Oliveira, A. L., Aghaei, M., & Rüther, R. (2022b). Automatic Inspection of Photovoltaic Power Plants Using Aerial Infrared Thermography: A Review. *Energies*, *15*(6), 2055. https://doi.org/10.3390/en15062055

[80] Augmentation des données. (n.d.). *TensorFlow*. https://www.tensorflow.org/tutorials/images/data_augmentation?hl=fr

[81] Sharma, D. (2023). Image Classification Using CNN | Step-wise Tutorial. *Analytics Vidhya*. https://www.analyticsvidhya.com/blog/2021/01/image-classification-using-convolutional-neural-networks-a-step-by-step-guide/

[82] Nick. (2021). Introduction to PVsyst: The Best Solar Design Software for 2021. *GSES International*. https://www.gsesinternational.com/introduction-to-pvsyst-the-best-solar-design-software-for-2021/

[83] Gross, M. (2023). What is PVsyst? Comprehensive Guide 2023. *Partner Engineering and Science, Inc.* https://www.partneresi.com/resources/articles/what-is-pvsyst-comprehensive-guide-2023/

[84] Wang, Z., Conrad Bovik, A., Rahim Sheikh, H., & P. Simoncelli, E. (2004). *Image Quality Assessment: From Error Visibility to Structural Similarity*. IEEE.